Available online at www.sciencedirect.com
ScienceDirect
Trans. Nonferrous Met. Soc. China 25(2015) 211−240
Transactions of Nonferrous Metals Society of China
www.tnmsc.cn

Alloy gene Gibbs energy partition function and equilibrium holographic network phase diagrams of Au_3Cu-type sublattice system

Youq-qing XIE[1,2,3], Yao-zhuang NIE[4], Xiao-bo LI[5], Hong-jian PENG[6], Xin-bi LIU[1,2,3]

1. School of Materials Science and Engineering, Central South University, Changsha 410083, China;
2. Powder Metallurgy Research Institute, Central South University, Changsha 410083, China;
3. State Key Laboratory of Powder Metallurgy, Central South University, Changsha 410083, China;
4. School of Physics and Electronics, Central South University, Changsha 410083, China;
5. School of Materials Science and Engineering, Xiangtan University, Xiangtan 411105, China;
6. School of Chemistry and Chemical Engineering, Central South University, Changsha 410083, China

Received 17 November 2014; accepted 8 January 2015

Abstract: Taking Au_3Cu-type sublattice system as an example, three discoveries have been presented. First, the fourth barrier to hinder the progress of metal materials science is that today's researchers do not understand that the Gibbs energy function of an alloy phase should be derived from Gibbs energy partition function constructed of alloy gene sequence and their Gibbs energy sequence. Second, the six rules for establishing alloy gene Gibbs energy partition function have been discovered, and it has been specially proved that the probabilities of structure units occupied at the Gibbs energy levels in the degeneracy factor for calculating configuration entropy should be degenerated as ones of component atoms occupied at the lattice points. Third, the main characteristics unexpected by today's researchers are as follows. There exists a single-phase boundary curve without two-phase region coexisting by the ordered and disordered phases. The composition and temperature of the top point on the phase-boundary curve are far away from those of the critical point of the Au_3Cu compound; At 0 K, the composition of the lowest point on the composition-dependent Gibbs energy curve is notably deviated from that of the Au_3Cu compounds. The theoretical limit composition range of long range ordered Au_3Cu-type alloys is determined by the first jumping order degree.

Key words: Au_3Cu compound; Au_3Cu-type sublattice system; alloy gene Gibbs energy partition function; equilibrium holographic network phase diagrams; systematic metal materials science

1 Introduction

In the first paper of a series articles for the FCC-based lattice Au−Cu system [1], we presented four philosophic propositions of system sciences. The first proposition is that "A diversity of structures of a system is attributed to the combination and arrangement of structural units in the basic structure unit sequences". We delivered an extensive definition of the gene sequence: the gene sequence is a basic structure unit sequence carrying a set of transmission information about structures and properties for determining the diversity of structures and properties of a system, which may be a biologic or non-biologic system. Therefore, to seek alloy gene (AG) sequences is the first important task for establishing the systematic metal materials science (SMMS) framework [2,3], and also the first barrier to hinder the progress of metal materials science. The AG sequences are the A_i^{Au}- and A_i^{Cu}-central characteristic atom sequences in the B_i^{Au}- and B_i^{Cu}-basic coordination cluster sequences for the FCC-based lattice Au−Cu system. Their potential energies ($\varepsilon_i^{Au}, \varepsilon_i^{Cu}$) and volumes ($v_i^{Au}, v_i^{Cu}$) sequences were obtained by the separated theory of potential energies and volumes of characteristic atoms. The electronic structures, physical properties and complete thermodynamic properties were obtained by valence bond theory and thermodynamics of characteristic crystals, respectively. These data were deposited into the AG-holographic information database.

Foundation item: Project (51071181) supported by the National Natural Science Foundation of China; Project (2013FJ4043) supported by the Natural Science Foundation of Hunan Province, China
Corresponding author: You-qing XIE; Tel: +86-731-88879287; E-mail: xieyouq8088@163.com
DOI: 10.1016/S1003-6326(15)63598-1

The second proposition is that "The diversity of properties of a system is attributed to contents and transmission mode of the information of basic structure unit sequences". Therefore, to seek transmission mode of AG-information is the second task for establishing the SMMS framework, and also the second barrier to hinder the progress of metal materials science. The transmission mode of AG-information is described by AG-Gibbs energy $\Omega(x,T,\sigma)$ - partition function, which consists of the AG-characteristic Gibbs energy transmission $G^*(x,T,\sigma)$ - partition function and AG-arranging (AGA) $g(x_i^{\mathrm{Au}}(x,T,\sigma),x_i^{\mathrm{Cu}}(x,T,\sigma))$ - degeneracy function.

"The complexity and entirety of a complex system are attributed to the multilevel of the structures and properties and to the various correlativities between different structural levels, between different properties and between structure and property". It is the third philosophic proposition of system sciences. The SMMS framework should be divided into three levels: 1) AG-theory to establish AG-holographic information database, which includes separated theory of potential energies and volumes of characteristic atoms (alloy genes), valence bond theory and thermodynamics of characteristic crystals [4−7]. 2) AGA-theory of alloy phases to establish AGA-holographic network information database, which includes AGA-crystallographics [8], AGA-valence bond theory [9−12] and AGA-thermodynamics of alloy phases [1,13,14]. 3) Alloy phase arranging (APA) theory of organizations, which includes APA-thermodynamics and APA-structure theory of alloy systems. "Properties are determined by structures, properties should be suitable for environments and environments change structures". The man's knowledge of relationships of structures, properties and temperature for alloys has been changed from single causality to systematic correlativity, due to the discoveries of alloy gene sequences and their information transmission modes, as well as establishments of the SMMS framework, holographic alloy positioning (HAP) system, and equilibrium holographic network phase (EHNP) diagrams.

In the second paper [13], we proposed the fourth proposition: "The system has not only the ability to keep structure stabilization against a changing environment, but also a mechanism to change structure for suiting variation in environments". Therefore, to seek atom movement mechanism is the third important task for establishing kinetics of alloy phase transformations, and also the third barrier to hinder the progress of metal materials science. Taking experimental path on disordering AuCuI ($A_8^{\mathrm{Au}}A_4^{\mathrm{Cu}}$) composed of A_8^{Au} and A_4^{Cu} stem alloy genes as an example, we presented three discoveries: 1) The ability of the AuCuI($A_8^{\mathrm{Au}}A_4^{\mathrm{Cu}}$) to keep structure stabilization against changing temperature is attributed to that the $\varepsilon_8^{\mathrm{Au}}$ and $\varepsilon_4^{\mathrm{Cu}}$ potential well depths greatly surpass their vibration energies, which leads to experimental path in subequilibrium state. 2) A new atom movement mechanism of AuCuI ($A_8^{\mathrm{Au}}A_4^{\mathrm{Cu}}$) to change structure for suiting variation in temperature is the "resonance activating-synchro alternating" of alloy genes, and it leads to heterogeneous nucleation and successive subequilibrium transitions. 3) There exists jumping order degree, which leads to the existence of jumping T_J-temperature and an unexpected so-called "retro-effect" about jumping temperature retrograde shift to lower temperatures upon the increasing heating rate [15−17].

In the third paper [14], taking $AuCu_3$-type sublattice system as an example, we presented three discoveries: 1) The third barrier to hinder progress of metal materials science is that researchers have got used to recognizing experimental phenomena of alloy phase transitions during extremely slow variation in temperature by equilibrium thinking mode and then to take miss knowledge of experimental phenomena as selected information for establishing so-called Gibbs energy function and so-called equilibrium phase diagram. 2) The EHNP-diagrams of $AuCu_3$-type sublattice system may be used to describe systematic correlativity of the composition−temperature-dependent alloy gene arranging structures and complete thermodynamic properties, and to be a standard for studying experimental subequilibrium order-disorder transition. 3) The main characteristics of these EHNP-diagrams have never been expected by today's researchers.

In the present work, taking Au_3Cu-type sublattice system as an example, we presented three discoveries: 1) The fourth barrier to hinder the progress of metal materials sciences is that today's researchers do not understand that a real Gibbs energy function of an alloy phase should be derived from corresponding AG-Gibbs energy partition function constructed of AG-sequence and their Gibbs energy sequence. 2) To establish AG-Gibbs energy partition function should obey six rules, which can make us to understand problematic essentials of the currently used alloy solution models in quantum mechanical abinitio calculations of (QMAC)-thermodynamics and calculation of phase diagrams (CALPHAD)-thermodynamics. 3) The main characteristics of equilibrium holographic network phase diagrams of the Au_3Cu-type sublattice system have never been expected by today's researchers, which may be used to explain some wondering experimental phenomena.

2 Rules for establishing AG-Gibbs energy partition function

In spite of a long history of statistical

thermodynamics [18−22], there is none of the currently used so-called Gibbs energy functions of alloy phases in QMAC- and CALPHAD-thermodynamics to be a real Gibbs energy function derived from the real Gibbs energy partition function. It shows that today's researchers do not understand that a real Gibbs energy function should be derived from the real Gibbs energy partition function constructed of the basic structure unit sequences and their Gibbs energy sequences. It is the fourth barrier to hinder the progress of the metal materials science, because some problems existed in these so-called Gibbs energy functions can not be easily overcome.

Based on the AG-Gibbs energy sequences and AGA-model, the AG-Gibbs energy partition function of the FCC-based lattice Au−Cu system has been established, which is used to describe the systematic correlativity of the AG-Gibbs energy levels ($G_i^{\mathrm{Au}}(T)$, $G_i^{\mathrm{Cu}}(T)$), AG-probabilities ($x_i^{\mathrm{Au}}(x,T,\sigma)$, $x_i^{\mathrm{Cu}}(x,T,\sigma)$) occupied at the AG-Gibbs energy levels and degeneracy $g(x_i^{\mathrm{Au}}(x,T,\sigma),x_i^{\mathrm{Cu}}(x,T,\sigma))$ factor of AG-probabilities as functions of the composition (x), temperature (T) and order degree (σ):

$$\Omega(x,T,\sigma)=g(x_i^{\mathrm{Au}}(x,T,\sigma),x_i^{\mathrm{Cu}}(x,T,\sigma))\times \exp[-G^*(x,T,\sigma)/(k_{\mathrm{B}}\mathrm{T})] \quad (1)$$

where k_{B} is the Boltzmann's constant, and $G^*(x,T,\sigma)$ is the characteristic Gibbs energy function of the alloy phase, which may be obtained by the transmission law of the AG-Gibbs energies:

$$G^*(x,T,\sigma)=\sum_{i=0}^{I=12}[x_i^{\mathrm{Au}}(x,T,\sigma)\times G_i^{\mathrm{Au}}(T)+ x_i^{\mathrm{Cu}}(x,T,\sigma)\times G_i^{\mathrm{Cu}}(T)] \quad (2)$$

The Gibbs energy function of the alloy phase may be derived from the $\Omega(x,T,\sigma)$ -function:

$$G(x,T,\sigma)=-k_{\mathrm{B}}T\times\ln(\Omega(x,T,\sigma))= G^*(x,T,\sigma)-TS^{\mathrm{c}}(x,T,\sigma) \quad (3)$$

The configurational entropy $S^{\mathrm{c}}(x,T,\sigma)$ -function is obtained from the degeneracy g-factor:

$$S^{\mathrm{c}}(x,T,\sigma)=k_{\mathrm{B}}\ln(g(x_i^{\mathrm{Au}}(x,T,\sigma),x_i^{\mathrm{Cu}}(x,T,\sigma))) \quad (4)$$

It should be pointed out that these functions may be suitable for Au_3Cu-, AuCu- and $AuCu_3$-type sublattice systems (σ>0), as well as disordered alloy phase (σ=0). However, their ordering definitions are different, of which the details can be seen from Ref. [23]. We have discovered six rules for establishing AG-Gibbs energy partition function, which may reveal problematic essentials of the currently used alloy solution models in the QMAC-thermodynamics [24] and the CALPHAD-thermodynamics [25−28].

1) "The structure units should be suited to alloy phase-structure level". An alloy phase is an alloy gene arranging (AGA) solution. The AG-sequences, AG-pair sequences and AG-cluster sequences may be used as structure unit sequences to establish Gibbs energy partition function, rather than "constituent atoms", "constituent atom pairs" and "constituent atom clusters". The AG-sequences carry structure information about coordinative configurations of theirs coordination clusters to describe diversity of AGA-phase structures and valences electron structures to explain essence of diversity of AGA-phase structures. However, the constituent units are not complete sequences with less information about only structures and properties of pure elements (see Appendix A.1).

2) "Energy level sequences should be AG-Gibbs energy sequences". The objects of the AG-Gibbs energy partition function of an alloy phase are to derive the AGA-Gibbs energy function and to obtain the equilibrium order-disorder transition $G_{\min}(x,T,\sigma)$ -path with minimum Gibbs energy of alloys as functions of composition, temperature and order degree, then to obtain equilibrium holographic network path (EHNP) charts of alloys and to establish EHNP-diagrams of alloy system, because each Gibbs energy level may be divided into two parts: a temperature-independent contribution of chemical potential energy(E(0)), of which the variation with temperature has been accounted in the attaching vibration energy, and a temperature- independent contribution of generalized vibration free energy $X^{\mathrm{v}}(T)$ level, which includes the generalized vibration energy $U^{\mathrm{v}}(T)$ and generalized vibration entropy $S^{\mathrm{v}}(T)$. The $U^{\mathrm{v}}(T)$ includes Debye vibration energy $U^{\mathrm{D}}(T)$ and attaching vibration energy $U^{\mathrm{E}}(T)$. The $S^{\mathrm{v}}(T)$ includes Debye vibration entropy ($S^{\mathrm{D}}(T)$) and attaching vibration entropy ($S^{\mathrm{E}}(T)$). The $U^{\mathrm{E}}(T)$ and $S^{\mathrm{E}}(T)$ include contributions of electron excitation, hole energy of formation, volume expansion work and variation in potential energy with temperature. If the generalized vibration free energy is neglected, the AG-Gibbs energy partition function becomes the AG-"potential energy" partition function [20], from which only the AGA-"potential free energy" function of alloy phases can be derived, then to obtain the so-called equilibrium order-disorder transition $E_{\min}$−T path with minimum "potential free energy" of the alloy. However, it may be proved that this alloy is not in equilibrium state, and it is minimal "potential energy $E_{\min}$-path is higher than the minimal Gibbs energy $G_{\min}$-path, because the negative value contributions of the AG-generalized vibration entropy energies surpass positive value contributions of the AG-generalized vibration entropy

energies to AG-Gibbs energies (see Appendixes A.2 and A.3). It is also demonstrated that the AG-probabilities occupied at the AG-potential energy levels in the equilibrium state should be calculated by the minimal Gibbs energy path method.

In the QMAC-thermodynamics, the effective cluster interaction parameters are obtained by fitting the $\Delta H^{\mathrm{m}}(0)$-enthalpy of formation, i.e., $\Delta E^{\mathrm{m}}(0)$-potential energy of formation, calculated from the first-principles at electron theory T=0 K, here, the generalized vibration free energy is neglected [29]. Consequently, only the potential free energy function can be obtained by this way.

In the CALPHAD-thermodynamics, the Gibbs energies of the pure elements are taken from the compilation of DINSDALE [30], and the excess Gibbs energies of the ordered and disordered alloy phases are modeled with a Gibbs energy expression in the compound energy formalism or in the form of a Redlich-Kister series, that contains a number of unknown parameters. These parameters may be adjusted until the Gibbs energy expression corresponding to the chosen model is capable of representing the selected information well [31]. Consequently, this so-called Gibbs energy function is questionable, based on the misunderstanding of that the middle jumping T_{j}-temperature is erroneously considered as the terminal T_{c}-critical temperature of order-disorder equilibrium transition.

3) "The Gibbs energy levels should be consistent with their structure units". In the Au−Cu system, the $Au_{(1-x)}Cu_x$ alloy may be defined as the "alloy gene arranging solution", where the A_i^{Au}- and A_i^{Cu}-alloy genes are regarded as the "structure units", which should be matched by "AG-Gibbs energy levels". The alloy may be also defined as the "alloy gene pair arranging solution", where the $A_i^{\mathrm{Au}}-A_{i'}^{\mathrm{Au}}$, $A_i^{\mathrm{Au}}-A_{i'}^{\mathrm{Cu}}$ and $A_i^{\mathrm{Cu}}-A_{i'}^{\mathrm{Cu}}$ alloy gene pairs are regarded as the "structure units", which should be matched by "alloy gene pair Gibbs energy levels". The alloy may be also defined as the "alloy gene cluster arranging solution", where the "alloy gene clusters" are regarded as the "structure units", which should be matched by "alloy gene cluster Gibbs energy levels". If the alloy is defined as the Au- and Cu-atom solution mixed by pure Au and Cu metals, where the Au- and Cu-atoms are regarded as the "constituent units". It is well known that after mixing Au- and Cu-pure elements, their energy states are split, so, there exist uncertain Gibbs energy levels to match them. Therefore, the QMAC and CALPHAD so-called Gibbs energy functions contain a number of unknown parameters, that may be understood from Appendixes A.2 and A.3.

4) "The used structure units should be the smallest ones". As compared with AG-pair and AG-cluster, the alloy gene is the smallest. The AG-Gibbs energy partition function and derived AGA-Gibbs energy function are simplest. It may be proved that if the AG-sequence, AG-pair sequence and AG-cluster sequence are the respectively complete sequences, the total Gibbs energies, characteristic Gibbs energies and configurational entropies calculated by them are identical. So, we should adopt the AG-sequence as the structure unit sequence, rather than AG-pair and AG-pair sequences for simplified calculation (see Appendixes A.2 and A.3). In the QMAC- and CALPHAD-thermodynamics, the atomic pairs and atomic clusters are the incomplete "constituent" units. The total Gibbs energies and configurational entropies calculated by different "constituent units" are different, respectively.

5) "A set of structure unit sequences with corresponding Gibbs energy sequences should be suitable for all phases in a based lattice system". The Au−Cu system with fcc-based lattice possesses a set of A_i^{Au}- and A_i^{Cu}-sequences with a set of G_i^{Au}- and G_i^{Cu}-sequences and other properties sequences, which may be suitable for describing Au_3Cu-, AuCu- and $AuCu_3$-type ordered phases, as well as disordered phase. Therefore, their Gibbs energy functions have no any adjustable parameters. The Al−Ni system with FCC- and BCC-based lattices possesses two sets of A_i^{Al}- and A_i^{Ni}-sequences. The Al−Ti system with FCC-, HCP and BCC-based lattices possesses three sets of A_i^{Al}- and A_i^{Ti}-sequences.

6) "The AG-probabilities occupied at the Gibbs energy levels should be degenerated by the probabilities of component atoms occupied at the sublattice points in the degeneracy function". In the AG-Gibbs energy partition function, the characteristic Gibbs energy $G^*(x,T,\sigma)$-function and degeneracy $g(x_i^{\mathrm{Au}}(x,T,\sigma), x_i^{\mathrm{Cu}}(x,T,\sigma))$-function are interrelated, because both they are associated with AG-propabilities occupied at the Gibbs energy levels. The relation of molar configurational entropy to degeneracy function is described by Boltzman's function (see Appendix A.4). Therefore, $S^{\mathrm{c}}(x,T,\sigma)$-function associated with the $G^*(x,T,\sigma)$-function is not independent contributor to Gibbs energy of the alloy phase.

In the fourth rule, it has been pointed out that the Gibbs energy, characteristic Gibbs energy and configurational entropies calculated respectively by AG-, AG-pair and AG-cluster sequences should be identical, if they are complete sequences and matched by their Gibbs energy sequences. It means that the calculated configurational entropies are independent on the sizes of structure units. We have also calculated configurational entropies by three degeneracy $g(x,T,\sigma)$-functions. It has been proved that the AG-probabilities occupied at the AG-Gibbs energy levels in the degeneracy function

should be degenerated by those of the constituent units occupied at the sublattice points, i.e., Bragg-William model [32,33] (see Appendix A.4), because the AG-generalized vibration entropy energy $TS_i^{\mathrm{v}}(T)$ has been accounted in the AG-Gibbs energy level (see Appendix A.2) .

In the QMAC- and CAPPHAD-thermodynamics, the configurational entropy is regarded as independent contributor to Gibbs energy and dependent on the sizes of constituent units, because the atomic pairs and atomic clusters are the incomplete constituent units.

3 EHNP-diagrams of Au_3Cu-type sublattice system

3.1 Steps for establishing EHNP-diagrams

An equilibrium order/disorder transition for a given composition alloy is defined as that "the AG-Gibbs energy levels ($G_i^{\mathrm{Au}}(T)$, $G_i^{\mathrm{Cu}}(T)$) and AG-probabilities ($x_i^{\mathrm{Au}}(x,T,\sigma)$, $x_i^{\mathrm{Cu}}(x,T,\sigma)$) occupied at the $G_i^{\mathrm{Au}}(T)$- and $G_i^{\mathrm{Cu}}(T)$-energy levels can respond immediately and change synchronously with each small variation in temperature and proceed along the minimal Gibbs energy path, supposing that there is no obstacle to atom movement". The man's knowledge of relationships of structures, properties and temperature for alloys has been changed from single causality to systematic correlativity, due to the discovery of alloy gene A_i^{Au}- and A_i^{Cu}- sequences and establishment of the AG-Gibbs energy partition function. The systematic correlativity of the Au_3Cu-type sublattice system may be described by a set of EHNP diagrams, which are obtained by following steps.

1) According to the $G_i^{\mathrm{Au}}(T)$ and $G_i^{\mathrm{Cu}}(T)$ level sequences, mixed Gibbs energy $\Delta G^{\mathrm{m}}(x,T,\sigma)$-function and essential definition of equilibrium order-disorder transition, the systematic correlativity of the $\Delta G_{\mathrm{e}}^{\mathrm{m}}-T$, $\sigma_{\mathrm{e}}-T$, $S_{\mathrm{e}}^{\mathrm{c}}-T$, $x_{i,\mathrm{e}}^{\mathrm{Au}}-T$ and $x_{i,\mathrm{e}}^{\mathrm{Cu}}-T$ paths on equilibrium order-disorder transition as function of temperature for the stoichiometric Au_3Cu-alloy are calculated by the minimal mixed Gibbs energy $\Delta G_{\mathrm{min}}^{\mathrm{m}}-T$ path method, which includes the iso-order degree Gibbs energy $\Delta G_{\sigma}^{\mathrm{m}}-T$ path method (Fig. 1(a)) and the isothermal Gibbs energy $\Delta G_{T}^{\mathrm{m}}-\sigma$ path method (Fig. 1(b)), using the calculated steps ΔT=1 K and $\Delta\sigma$=0.0001. According to the $x_{i,\mathrm{e}}^{\mathrm{Au}}-T$ and $x_{i,\mathrm{e}}^{\mathrm{Cu}}-T$ paths, the EHNP charts of the stoichiometric Au_3Cu-alloy are calculated and shown in Appendix B.

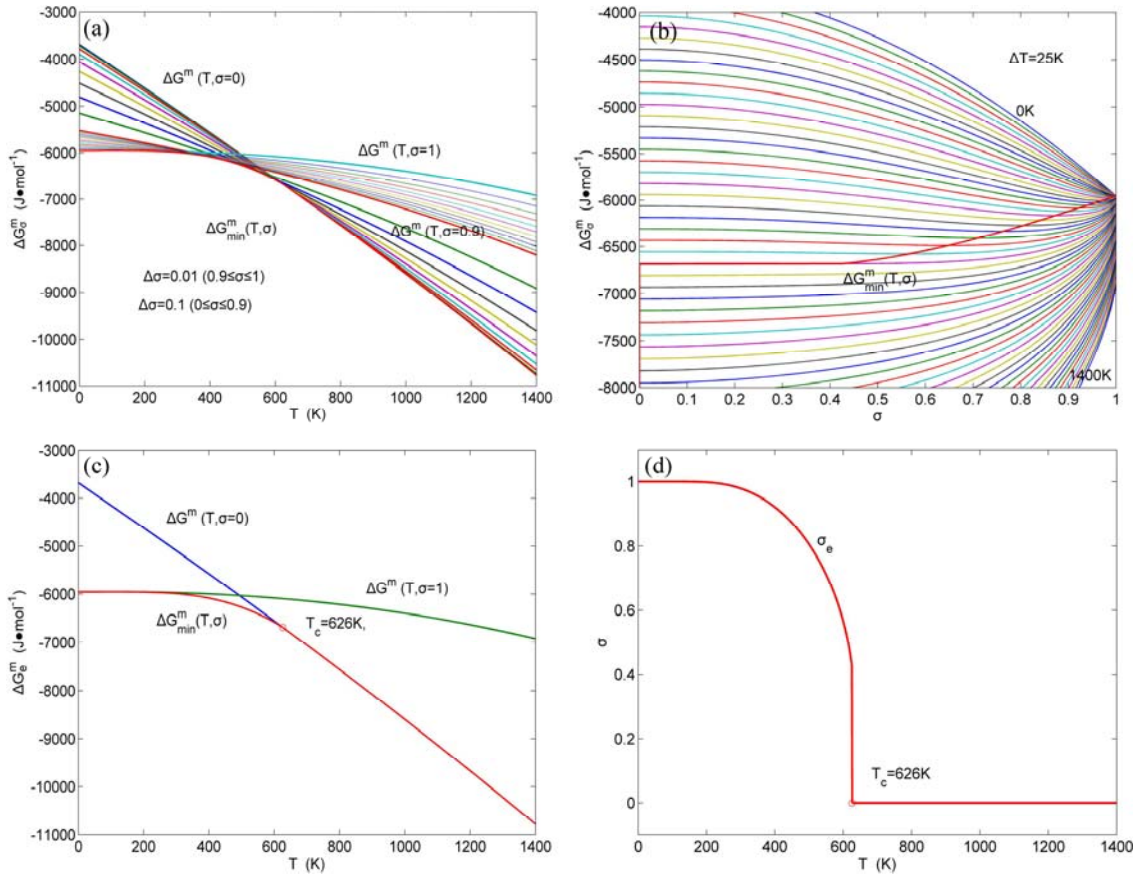

Fig. 1 Minimal mixed Gibbs energy $\Delta G_{\mathrm{min}}^{\mathrm{m}}-T$ path on equilibrium order-disorder transition of stoichiometric Au_3Cu alloy: (a) Iso-order degree Gibbs energy $\Delta G_{\sigma}^{\mathrm{m}}-T$ path method; (b) Isothermal Gibbs energy $\Delta G_{T}^{\mathrm{m}}-\sigma$ path method; (c) $\Delta G_{\mathrm{e}}^{\mathrm{m}}(\Delta G_{\mathrm{min}}^{\mathrm{m}})-T$ path on equilibrium order/disorder transition of stoichiometric Au_3Cu alloy; (d) σ−T path on equilibrium order/disorder transition of stoichiometric Au_3Cu alloy

2) By analogy with the first step, the systematic correlativity data of the $\Delta G_{\mathrm{e}}^{\mathrm{m}}(x,T)$, $\sigma_{\mathrm{e}}(x,T)$, $S^{\mathrm{c}}(x,T)$, $x_{i,\mathrm{e}}^{\mathrm{Au}}(x,T)$ and $x_{i,\mathrm{e}}^{\mathrm{Cu}}(x,T)$ paths on equilibrium order−disorder transition as function of composition and temperature for all alloys of the Au_3Cu-type sublattice system are calculated, using calculated steps Δx=0.5%, ΔT=1 K, $\Delta\sigma$=0.0001.

3) According to the systematic correlativity data of the $\Delta G_{\mathrm{e}}^{\mathrm{m}}(x,T)$, $\sigma_{\mathrm{e}}(x,T)$, $S^{\mathrm{c}}(x,T)$, $x_{i,\mathrm{e}}^{\mathrm{Au}}(x,T)$ and $x_{i,\mathrm{e}}^{\mathrm{Cu}}(x,T)$, the three-dimensional $\Delta G_{\mathrm{e}}^{\mathrm{m}}-x-T$, $\sigma_{\mathrm{e}}-x-T$, $S_{\mathrm{e}}^{\mathrm{c}}-x-T$, $x_{i,\mathrm{e}}^{\mathrm{Au}}-x-T$ and $x_{i,\mathrm{e}}^{\mathrm{Cu}}-x-T$ EHNP diagrams, as well as their two-dimensional q_x-T, T_q-x and q_T-x path network phase diagrams and configuration entropy EHNP diagrams are constructed and shown in Figs. 2−5.

4) According to the first order thermodynamic properties in the AG-database and $x_{i,\mathrm{e}}^{\mathrm{Au}}-x-T$ and $x_{i,\mathrm{e}}^{\mathrm{Au}}-x-T$ EHNP diagrams, the EHNP diagrams of the first order thermodynamic properties of the Au_3Cu-type sublattice system are calculated by their transmission laws, which may be also called as the additive law of extensive q-properties of characteristic crystals [1,34]. q denotes characteristic Gibbs energy (G^*), enthalpy (H), potential energy (E), volume (V), generalized vibration free energy (X^{v}), generalized vibration energy (U^{v}), generalized vibration entropy (S^{v}).

5) The EHNP diagrams of the second order thermodynamic properties (mixed heat capacity and mixed volume expansion coefficient) are calculated [1,13].

6) The EHNP diagrams of the activities of the Au- and Cu-components are calculated [1,13].

7) The composition−temperature-dependent $\Delta G_{\mathrm{PB}}^{\mathrm{m}}-x-T$, $(x_{i,\mathrm{e}}^{\mathrm{Au}})_{\mathrm{PB}}-x-T$ and $(x_{i,\mathrm{e}}^{\mathrm{Cu}})_{\mathrm{PB}}-x-T$ phase boundary (PB) curves are calculated by difference method of Gibbs energies between ordered and disordered phases (Appendix C)

8) According to the $(x_{i,\mathrm{e}}^{\mathrm{Au}})_{\mathrm{PB}}-x-T$ and $(x_{i,\mathrm{e}}^{\mathrm{Cu}})_{\mathrm{PB}}-x-T$ phase boundary curves, the other $q_{\mathrm{PB}}-x-T$ phase boundary curves are calculated.

3.2 Mixed Gibbs energy EHNP diagrams

The mixed Gibbs energy EHNP diagrams include a three-dimensional $\Delta G^{\mathrm{m}}-x-T$ network phase diagram and three two-dimensional $\Delta G_x^{\mathrm{m}}-T$, $T_{\Delta G^{\mathrm{m}}}-x$ and $\Delta G_T^{\mathrm{m}}-x$ path network phase diagrams (Fig. 2). In these diagrams, once one network point $(x,T,\Delta G^{\mathrm{m}})$ has been clicked, the information about composition (x), temperature (T) and mixed Gibbs energy (ΔG^{m}) may be readily obtained.

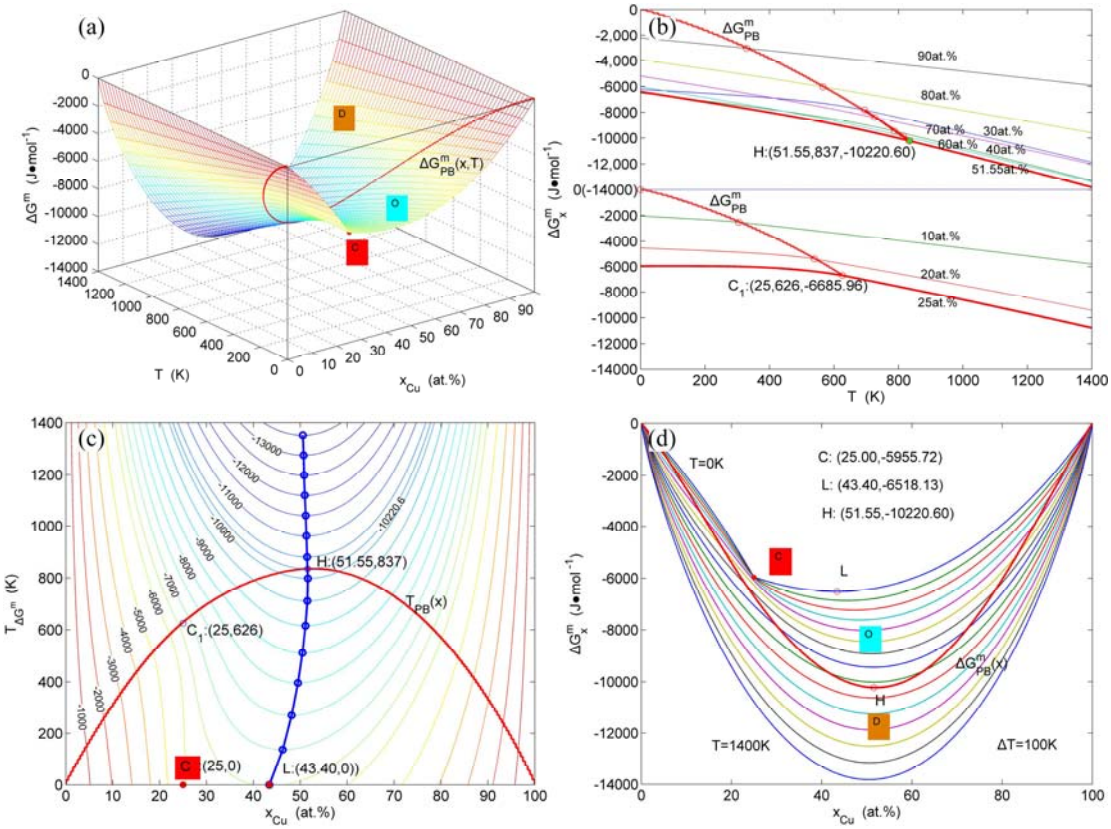

Fig. 2 Mixed Gibbs energy EHNP diagrams of Au_3Cu-type sublattice system: (a) Three-dimensional $\Delta G^{\mathrm{m}}-x-T$ diagram with phase boundary curve $\Delta G_{\mathrm{PB}}^{\mathrm{m}}(x,T)$; (b) Two-dimensional isocompositional $\Delta G_x^{\mathrm{m}}-T$ path diagram with phase boundary curve $\Delta G_{\mathrm{PB}}^{\mathrm{m}}(T)$; (c) Two-dimensional iso-mixed Gibbs energy $T_{\Delta G^{\mathrm{m}}}-x$ diagram with phase boundary curve $T_{\mathrm{PB}}(x)$; (d) Two-dimensional isothermal $\Delta G_{\mathrm{T}}^{\mathrm{m}}-x$ diagram with phase boundary curve $\Delta G_{\mathrm{PB}}^{\mathrm{m}}(x)$

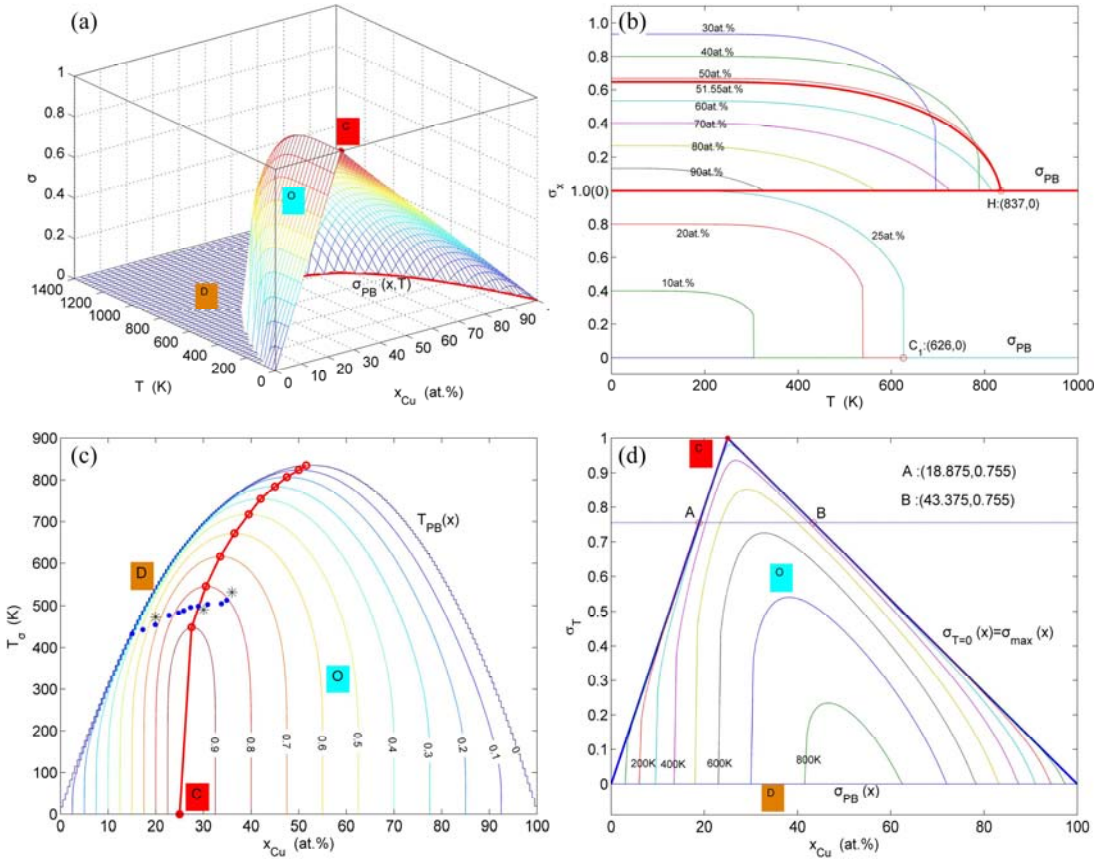

Fig. 3 Order degree EHNP diagrams of Au_3Cu-type sublattice system: (a) Three-dimensional $\sigma-x-T$ diagrams with phase boundary curve $\sigma_{PB}(x,T)$; (b) Two-dimensional isocompositional σ_x-T path diagrams with phase boundary curve $\sigma_{PB}(T)$; (c) Two-dimensional iso-order degree $T_\sigma-x$ diagrams with phase boundary curve $T_{PB}(x)$; (d) Two-dimensional isothermal σ_T-x diagram with phase boundary curve $\sigma_{PB}(x)$

From Fig. 2(a), the following main understandings may be obtained. 1) There are ordered single-phase region with Gibbs energy network points (denoted by the symbol "O") and disordered single-phase region with Gibbs energy network points (denoted by the symbol "D"). 2) The $\Delta G^{m}_{PB}(x,T)$-phase boundary (PB) curve with Gibbs energy network points is obtained by difference method of Gibbs energies between ordered and disordered phases. By this method, it has been proved that there is a single-phase boundary curve rather than a boundary two-phase region of ordered and disordered phases: 3) The equilibrium state of the stoichiometric Au_3Cu compound, of which the alloy gene arranging (AGA)-molecular formula is the $(A_4^{Au})_3A_0^{Cu}$, exists only at the network C-point (x_{Cu}=25%, T=0 K, ΔG^{m}=−5955.72 J/mol).

From Fig. 2(b), the following main understandings may be obtained. 1) The critical network point, i.e., phase boundary point, of the stoichiometric Au_3Cu alloy, is located at the network C_1-point (x_{Cu}=25%, T_c=626 K, ΔG^{m}=−6685.96 J/mol). 2) The $Au_{48.35}Cu_{51.65}$ alloy has the highest critical temperature in the Au_3Cu-type sublattice system, it is located at the network H-point (x_{Cu}=51.55%, T_c=837 K, ΔG^{m}=−10220.60 J/mol). 3) The equilibrium $\Delta G^{m}_{x,e}-T$ path for a given composition (x) alloy is the standard path for determining Gibbs energy hysteresis effect, i.e., superheated and undercooled driving Gibbs energies ($\Delta G^{m}_{x,e}(T)-\Delta G^{m}_{x,s}(T)$) of experimental $\Delta G^{m}_{x,s}(T)-$path.

From Fig. 2(c), we can know that the lowest network points of the iso-mixed Gibbs energy $T_{\Delta G^m}-x$ curves move from the network L-point (x_{Cu}=43.40%, T=0 K, $\Delta G^{m}=\Delta E^{m}$=−6518.13 J/mol) to the network H-point (x_{Cu}=51.55%, T_c=837 K, ΔG^{m}=−10220.60 J/mol), that is unexpected by today's researchers.

From Fig. 2(d), we can know that the $Au_{56.60}Cu_{43.40}$ alloy with the lowest potential energy is located at the network L-point, which notably deviates from the C-point, that is also unexpected by today's researchers. This diagram will be used to establish EHNP diagrams of the Au−Cu system together with isothermal $\Delta G^{m}_{T}-x$ diagrams of the AuCu-type and $AuCu_3$-type sublattice systems.

3.3 Order degree EHNP diagrams

The order degree EHNP diagrams include a

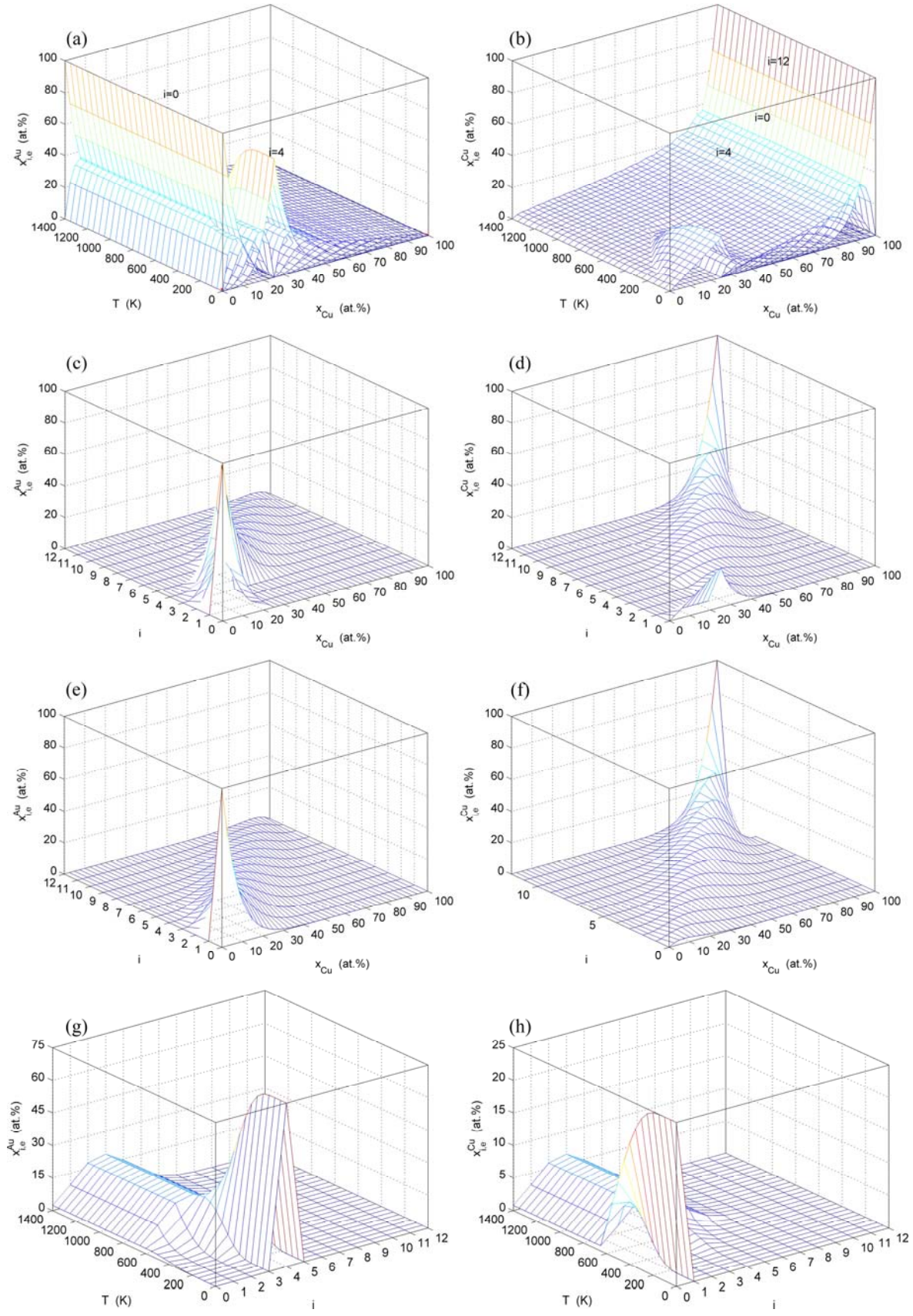

Fig. 4 AG-concentration EHNP diagrams: (a, b) Three-dimensional $x_{i,\mathrm{e}}^{\mathrm{Au}}-x-T$ and $x_{i,\mathrm{e}}^{\mathrm{Cu}}-x-T$ diagrams; (c, d) Three-dimensional $x_{i,\mathrm{e}}^{\mathrm{Au}}-x-i$ and $x_{i,\mathrm{e}}^{\mathrm{Cu}}-x-i$ diagrams of ordered $\mathrm{Au}_{(1-x)}\mathrm{Cu}_x$ alloys with maximum order degree $\sigma_{\max}$ at 0 K; (e, f) Three-dimensional $x_{i,\mathrm{e}}^{\mathrm{Au}}-x-i$ and $x_{i,\mathrm{e}}^{\mathrm{Cu}}-x-i$ diagrams of perfectly disordered $\mathrm{Au}_{(1-x)}\mathrm{Cu}_x$ alloys; (g, h) Three-dimensional $x_{i,\mathrm{e}}^{\mathrm{Au}}-T-i$ and $x_{i,\mathrm{e}}^{\mathrm{Cu}}-T-i$ path charts on disordering or ordering stoichiometric $\mathrm{Au_3Cu}$ alloy

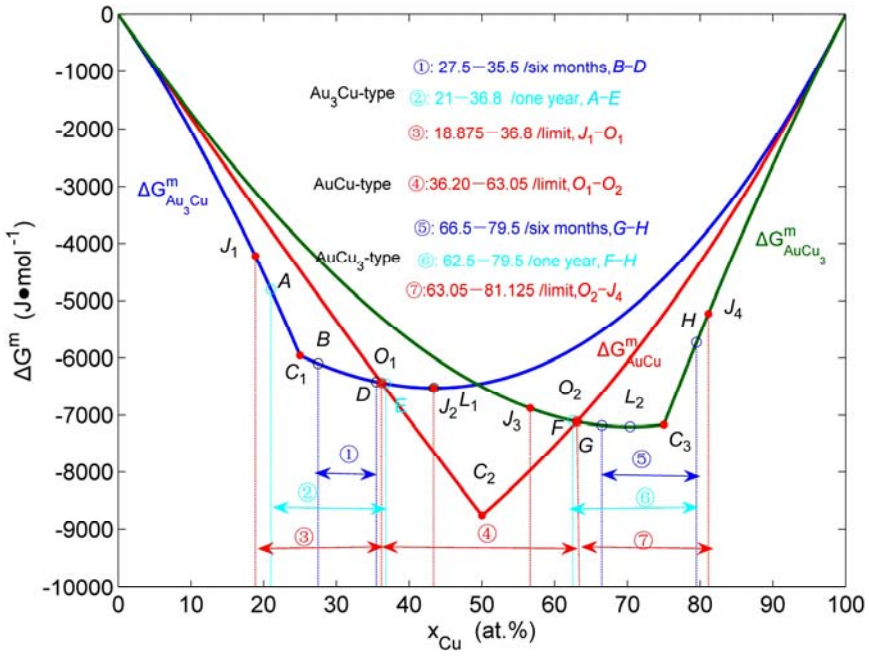

Fig. 5 Characteristics of $\Delta G^{\mathrm{m}}_{\mathrm{Au_3Cu}}-x$, $\Delta G^{\mathrm{m}}_{\mathrm{AuCu}}-x$ and $\Delta G^{\mathrm{m}}_{\mathrm{Au_3Cu}}-x$ curves of Au_3Cu-type, AuCu-type and $AuCu_3$-type sublattice systems (Each point is described by composition, mixed Gibbs energy and order degree: J_1(18.875, −4220.47, 0.0.7540), A(21.00, −4807.10, 0.8400, C_1(25.00, −5955.72, 1), B(27.50, −6094.93, 0.9667), D(35.50, −6411.03, 0.8600), O_1(36.20, −6428.97, 0.8507), E(36.80, −6443.06, 0.8427), J_2(43.375, −6518.13, 0.7553), L_1(43.40, −6518.13, 0.7547), C_2(50, −8746.23, 1), J_3(56.625, 0.7547), F(62.50, −7094.10, 0.8333), O_2(63.05, −7108.69, 0.8407), G(66.50, −7176.61, 0.8667), L_2(70.35, −7203.16, 0.9380), C_3(75, −7163.61, 1), H(79.50, −5726.05, 0.8200), J_4(81.125, −5320.59, 0.7550)

three-dimensional $\sigma-x-T$ network phase diagram and three two-dimensional σ_x-T, $T_\sigma-x$ and σ_T-x path network phase diagrams (Fig. 3). In these diagrams, once one network point has been clicked, the information about composition (x), temperature (T) and order degree (σ), as well as the mixed Gibbs energy (ΔG^{m}) may be readily obtained, because the order degree EHNP diagrams have been attached to the mixed Gibbs energy EHNP diagrams.

From Fig. 3(a), the following main understandings may be obtained. 1) There are ordered phase region with order degree network points (denoted by the symbol "O", σ>0), disordered phase region (denoted by the symbol "D", σ=0) and $\sigma_{\mathrm{PB}}(x,T)$-phase boundary (PB) curve (σ=0). 2) The equilibrium state of the $(A_4^{\mathrm{Au}})_3A_0^{\mathrm{Cu}}$ compound exists only at the network C-point (x_{Cu}=25%, T=0 K, σ=1).

From Fig. 3(b), we can know that: 1) The equilibrium $\sigma_{x,\mathrm{e}}-T$ paths of alloys on the Au-rich side of the $(A_4^{\mathrm{Au}})_3A_0^{\mathrm{Cu}}$ compound have great difference from thoes of alloys on the Cu-rich side of the $(A_4^{\mathrm{Au}})_3A_0^{\mathrm{Cu}}$ compound. 2) The $Au_{48.45}Cu_{51.55}$ alloy in the single Au_3Cu-type sublattice system has the highest critical temperature, and its network H-point (x_{Cu}=51.55%, T_{c}=837 K, σ=0) deviates far from the network C_1-point (x_{Cu}=25%, T_{c}=626 K, σ=0) of stoichiometric Au_3Cu alloy. However, their network points are respectively (x_{Cu}=51.55%, σ=0.64) and (x_{Cu}=25%, σ=1) at 0 K. 3) The equilibrium $\sigma_{x,\mathrm{e}}-T$ path for a given composition (x) alloy is the standard path for studying subequilibrium $\sigma_{x,\mathrm{s}}-T$ paths. These phenomena can not be expected in the QMAC- and CALPHAD-thermodynamics.

From Fig. 3(c), we have discovered surprising phenomena: All experimental middle jumping T_{j}-temperatures (denote by symbols "·" and "*" introduced from Ref. [35], which were erroneously considered as the so-called T_{c}-critical temperatures of equilibrium order-disorder transition of alloys, approach to equilibrium iso-order degree $T_{\sigma=0.8}-x$ curve.

Figure 3(d) shows that the network points of alloys with jumping-phenomena of order-disorder transition should be situated in the range from A-point to B-point, i.e., 0.755≤σ≤1 and 18.875%≤x_{Cu}≤43.375%.

3.4 AG-concentration EHNP diagrams

From Fig. 4, the following main understandings may be obtained. 1) The AG-concentration EHNP diagrams, which are used to describe the AGA-structures of alloy phases, may be described by two modes: three-dimensional $x_i^{\mathrm{Au}}-x-T$ and $x_i^{\mathrm{Cu}}-x-T$ network phase diagrams (Figs. 4(a) and (b)) in the AGA-crystallography (see Appendix A.1), where the x_i^{Au} and x_i^{Cu} are the probabilities occupied at the lattice points;

three-dimensional $x_i^{Au}-x-i$ and $x_i^{Cu}-x-i$ network phase diagrams (Figs. 4(c) and (d)) in the AGA-Gibbs energy level theory, where the x_i^{Au} and x_i^{Cu} are the probabilities occupied at the $G_i^{Au}(T)$ and $G_i^{Cu}(T)$ energy levels. 2) There exists an emergent phenomenon of some AG-concentrations in the ordered alloy phases, which are defined as that some AG-concentrations in the ordered state are larger than those in disorder state, such as x_4^{Au}, x_5^{Au}, x_0^{Cu} and x_1^{Cu} (Figs. 4(c), (d), (e) and (f)). 3) The equilibrium $x_{i,e}^{Au}-T$ and $x_{i,e}^{Cu}-T$ paths for a given composition (x) alloy may be described by three-dimensional $x_i^{Au}-x-i$ and $x_i^{Cu}-x-i$ equilibrium path charts (Figs. 4(g) and (h)) or two-dimensional $(x_i^{Au})_\sigma-i$ and $(x_i^{Cu})_\sigma-i$, as well as $x_i^{Au}-\sigma$ and $x_i^{Cu}-\sigma$ equilibrium path charts. The essential on disordering $(A_4^{Au})_3A_0^{Cu}$ compound is that the A_4^{Au} and A_0^{Cu} stem alloy genes are split into A_i^{Au} and A_i^{Cu} sequences in the disordered state. 4) It can be known that each kind of q-EHNP diagram includes not only the four type diagrams indicated above, but also other type diagrams. These AG-concentration equilibrium path charts will provide standard path charts for studying kinetic mechanism of experimental subequilibrium order-disorder transition path.

3.5 EHNP diagrams of other thermodynamic properties

According to $x_i^{Au}-x-T$ and $x_i^{Cu}-x-T$ EHNP diagrams obtained from ΔG^m-x-T diagram, we have obtained q−x−T EHNP diagrams of other thermodynamic properties of Au_3Cu-type sublattice system, which are shown in Appendix C. It should be emphasized that from each three-dimensional q−x−T EHNP diagram, we can obtain isocompositional q_x-T, isoproperty T_q-x and isothermal q_T-x path phase diagrams. The diagrams from Section 3.3 through present section are interconnected to form a big holographic network information database about structures, properties and their variations in composition and temperature of alloys. Therefore, the man's knowledge of relationships of structures, properties and environments for alloys has been changed from single causality to systematic correlativity. Once one network point in any EHNP diagram above has been clicked, the information about composition, temperature, order degree, AGA-structure and a set of thermodynamic properties of the alloy as well as its equilibrium order-disorder transition EHNP charts may be readily obtained, which are very useful for materials engineers to design advanced alloys.

4 Discussion

4.1 Gibbs energies of stoichiometric compounds

It seems to be a fundamental concept prevailing in QMAC- and CALPHAD-thermodynamics that a stoichiometric compound should have the lowest Gibbs energy and highest critical temperature in its ordered sublattice system. From Fig. 5, it can be known that the lowest points on the ΔG_{AuCu}^m-x, $\Delta G_{AuCu_3}^m-x$ and $\Delta G_{Au_3Cu}^m-x$ curves are respectively the L_2-point, which is exactly equal to C_2-point of the stoichiometric $AuCu(A_8^{Au}A_4^{Cu})$ compound, the L_3-point, which is slightly deviated from the C_3-point of the stoichiometric $AuCu_3(A_{12}^{Au}(A_8^{Cu})_3)$ compound, and the L_1-point, which is notably deviated from the C_1-point of the stoichiometric $Au_3Cu((A_4^{Au})_3A_0^{Cu})$ compound. These calculated results have never been obtained by researchers in the QMAC- and CALPHAD-communities. From their calculated phase diagrams, it can be known that they have consistently thought that stoichiometric Au_3Cu compound should have the lowest Gibbs energies and highest critical temperatures in their ordered sublattice systems [14,25−27,36].

4.2 Some unexpected phenomena

In an extensive X-ray investigation of the Au−Cu system performed by LU and LIANG [37−39], some wondering phenomena were obtained, that may be explained as follows (see Fig. 5).

1) The composition range of the ordered Au_3Cu-type alloys varies with annealing times. Under the experimental condition of six months of heat treatment, the composition range is ①: B−D, which does not include the stoichiometric Au_3Cu compound. This wondering phenomenon has been predicated by our research results. From Fig. 5, it can be known that, the ①: B−D range is included in the theoretical limit range J_1−J_2 (18.875%−43.375% Cu) of long range order (LRO) Au_3Cu-type alloys, which is determined by the first jumping order degree (0.755) of the jumping A_5^{Au}-alloy gene (see Fig. 3(d)); the lowest composition L_1-point on the $\Delta G_{Au_3Cu}^m-x$ curve is notably deviated from the C_1-point of the stoichiometric Au_3Cu compound; it possesses higher Gibbs energy than the alloys in the ①: B−D range, and the reaction rate is very slow as well.

2) Under the experimental condition of one year of heat treatment, the composition range is ②: A−E, which includes the stoichiometric Au_3Cu compound. Here, the lower composition B-point reaches the A-point, which is near to the composition J_1-limit; the upper composition E-point reaches the cross O_1-point of the $\Delta G_{Au_3Cu}^m-x$ and ΔG_{AuCu}^m-x curves, which is far away from the upper composition J_2-limit determined by the Au_3Cu-type sublattice system, due to the stop of the AuCu-type sublattice system. We may also predicate that if increasing the time of heat treatment, the lower composition point would move more close to the lower

composition J_1-limit, but the upper composition point would not move, due to the existence of the AuCu-type sublattice system with lower $\Delta G^{m}_{AuCu}-x$ curve.

3) According to analogous analysis, we have predicated that the theoretical limit composition range of the LRO-$AuCu_3$-type alloys in the single $AuCu_3$-type sublattice system should be from J_3-point to J_4-point [14], and its limit composition range in the Au−Cu system should be from the O_2-point to J_4-point, where the O_2-point is the cross point of the $\Delta G^{m}_{AuCu_3}-x$ and $\Delta G^{m}_{AuCu}-x$ curves (see Fig. 5); as well as that the lowest L_2-point on the $\Delta G^{m}_{AuCu_3}-x$ curve at 0 K is near to the C_3-point. These predicated results are in good agreement with the experiment phenomena (see Fig. 6).

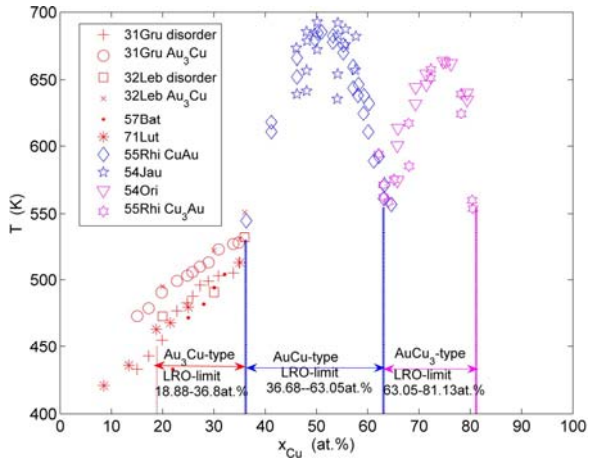

Fig. 6 Limit composition ranges of long range ordered Au_3Cu-type, AuCu-type and $AuCu_3$-type alloys in Au−Cu system determined by their first jumping order degrees together with experimental jumping points, which are introduced from Ref. [25]

4) Figure 5 shows that the C_1−C_2 and C_2−C_3 composition ranges are respectively the theoretical equilibrium of two phase regions between the ordered Au_3Cu-type and AuCu-type phases and between the ordered AuCu-type and $AuCu_3$-type phases. However, the experimental measurements show that the two-phase coexistences disappear after one year's treatment. Therefore, the experimental single Au_3Cu-type alloys in the C_1−O_1 range, single AuCu-type alloys in the O_1−O_2 range and single $AuCu_3$-type alloys in the O_2−C_3 range are really in a metastable state.

5) Finally, the experimental measurements show that there exist no two-phase regions between the ordered Au_3Cu-type phase and the disordered phase and between the ordered $AuCu_3$-type phase and the disordered phase at room temperature, that has been demonstrated by difference method of Gibbs energies between ordered and disordered phases (see Appendix B).

5 Conclusions

1) Based on the AG-holographic information database and essential definition of equilibrium order-disorder transition, the EHNP-diagrams of the Au_3Cu-type sublattice have been established by the minimal mixed Gibbs energy path method. These diagrams exhibit unexpected characteristics of equilibrium transition of Au_3Cu-type sublattice system, and may be used as a standard for studying experimental subequilibrium transition. Once one network point has been clicked, the information about the composition, temperature, AG-concentrations, holographic properties and EHNP-charts of the alloy may be readily obtained. These achievements will prove stimulating to materials engineers, and who may well find value in using it as a big information database for materials discovery, design, manufacture and application.

2) To establish AG-Gibbs energy partition function should obey six rules, which can make us to understand problematic essentials of the currently used alloy solution models in the QMAC-thermodynamics and CALPHAD-thermodynamics.

3) It has been proved that the AG-generalized vibration entropy energy $TS_i^{v}(T)$ is always larger than the AG-generalized vibration energy $U_i^{v}(T)$ and that the AG-probabilities occupied at the AG-Gibbs energy levels in the degeneracy function for calculating configurational entropy should be degenerated by thoes of the constituent units occupied at the sublattice points, i.e., Bragg-William model.

4) In the Au−Cu system, the experimental lower limit composition of the LRO-Au_3Cu-type alloys is determined by the first jumping order degree, and its upper limit composition is determined by the cross point of the $\Delta G^{m}_{Au_3Cu}-x$ and $\Delta G^{m}_{AuCu}-x$ curves at 0 K; the experimental lower limit composition of the LRO-$AuCu_3$-type alloys is determined by the cross point of the $\Delta G^{m}_{AuCu}-x$ and $\Delta G^{m}_{AuCu_3}-x$ curves at 0 K, and its upper limit composition is determined by the first jumping order degree, and the experimental lower limit composition range of the LRO-AuCu-type alloys is determined by two cross points above. However, the heat treatment conditions and heating rates have great influence on jumping temperatures.

5) Today's researchers in metallic materials science and physics do not understand that a real Gibbs energy function should be derived from the real Gibbs energy partition function constructed of the basic structure unit sequences and their Gibbs energy sequences. It is the fourth barrier to hinder the progress of the metal materials science, because some problems existed in these so-called Gibbs energy functions can not be easily

overcome and the reductionism is still in the dominate position.

Appendixes

A Explanations of rules for establishing alloy gene Gibbs energy parathion function

A.1 Explanation of constituent units and structure units

In the traditional crystallography of alloy phases, the smallest representative of a crystal is a cell, which is described by taking symmetry elements to operate constituent atoms as structure units. Therefore, it may be named the constituent atom arranging (CAA) structure of alloy phase. Table A.1 shows the CAA-structure of the Au- and Cu-pure metals and alloy phases. In the Au- and Cu-pure metals, stoichiometric AuCu-, $AuCu_3$- and Au_3Cu-compounds, AuCu-type, $AuCu_3$-type and Au_3Cu-type ordered alloys, as well as disordered alloys, all lattice points are occupied by Au- and Cu-constituent atoms. We can not know their information about coordinative configurations, electronic structures, potential energies, vibration energies and volumes, as well as other properties. Therefore, the Au- and Cu-constituent atoms belong in degenerated atoms respectively by the A_i^{Au}- and A_i^{Cu}- characteristic atoms and incomplete sequences with less information about only properties of Au- and Cu-pure metals and some unknown energetic parameters. The Au- and Cu-pure metals belong in degenerated crystals respectively by the C_i^{Au}- and C_i^{Cu}- characteristic crystals. Therefore, the alloy may be defined as the CAA-solution.

In the AGA-crystallography of the SMMS framework, the crystalline cell is described by taking symmetry elements operate alloy genes (i.e., characteristic atoms) as structure unit sequences. Table A.2 gives the AGA-structures of the Au- and Cu-pure metals, stoichiometric AuCu-, $AuCu_3$- and Au_3Cu-compounds, AuCu-type, $AuCu_3$-type and Au_3Cu-type ordered alloys, as well as disordered alloys. The lattice points are occupied by A_i^{Au}- and A_i^{Cu}- characteristic atoms. We can know their information about coordinative configurations, electronic structures, potential energies, vibration energies and volumes, as well as other properties [1]. The AGA-cells and potential wave planes of the AuCu-, $AuCu_3$- and Au_3Cu-compounds are shown in Fig. A.1 [39]. Therefore, the alloy may be defined as the AGA-solution.

A.2 Generalized vibration free energy and generalized vibration entropy energy

It has been proved that the AG-generalized vibration free energy $X_i^{\mathrm{v}}(T)$ always is negative, because the generalized vibration entropy energy $TS_i^{\mathrm{v}}(T)$ is always larger than the generalized vibration energy $U_i^{\mathrm{v}}(T)$.

The contributions of AG-generalized vibration energies and AG-generalized vibration entropy energies to AG-Gibbs energies. The AG-Gibbs energy is a complex function with multi-energetic levels:

$$G_i^{\alpha}(T)=E_i^{\alpha}(0)+X_i^{\alpha.\mathrm{v}}(T)=H_i^{\alpha}(T)-TS_i^{\alpha.\mathrm{v}}(T) \quad (1)$$

$$X_i^{\alpha.\mathrm{v}}(T)=U_i^{\alpha.\mathrm{v}}(T)-TS_i^{\alpha.\mathrm{v}}(T) \quad (2)$$

$$H_i^{\alpha}(T)=E_i^{\alpha}(0)+U_i^{\alpha.\mathrm{v}}(T) \quad (3)$$

$$X_i^{\alpha.\mathrm{D}}(T)=U_i^{\alpha.D}(T)-TS_i^{\alpha.\mathrm{D}}(T) \quad (4)$$

$$X_i^{\alpha.\mathrm{E}}(T)=U_i^{\alpha.\mathrm{E}}(T)-TS_i^{\alpha.\mathrm{E}}(T) \quad (5)$$

$$U_i^{\alpha.\mathrm{v}}(T)=U_i^{\alpha.\mathrm{D}}(T)+U_i^{\alpha.\mathrm{E}}(T) \quad (6)$$

Table A.1 CAA-crystal structures of alloy phases in Au−Cu system

Phase	Basic lattice	Constituent atom at lattice site	Constituent atom arrangement cell	Space group
Pure Au	FCC-latticE	Au	[4Au]	*Fm*3*m*
Pure Cu	FCC-lattice	Cu	[4Cu]	*Fm*3*m*
AuCu compounds	Au(1) sublattice, Cu(2) sublattice	Au(1), Cu(2)	[2Au(1), 2Cu(2)]	*P*4/*mmm*
$AuCu_3$ compounds	Au(1) sublattice, Cu(2) sublattice	Au(1), Cu(2)	[Au(1), 3Cu(2)]	*Pm*3*m*
Au_3Cu compounds	Au(1) sublattice, Cu(2) sublattice	Au(1), Cu(2)	[3Au(1), Cu(2)]	*Pm*3*m*
AuCu-type ordered alloy	Au(1)-rich sublattice, Cu(2) -rich sublattice	(x_{Au}(1)Au+x_{Cu}(1)Cu), (x_{Au}(2)Au+x_{Cu}(2)Cu)	[2(x_{Au}(1)Au+x_{Cu}(1)Cu), 2(x_{Au}(2)Au+x_{Cu}(2)Cu)]	*P*4/*mmm*
$AuCu_3$-type ordered alloy	Au(1)-rich sublattice, Cu(2) -rich sublattice	(x_{Au}(1)Au+x_{Cu}(1)Cu), (x_{Au}(2)Au+x_{Cu}(2)Cu)	[(x_{Au}(1)Au+x_{Cu}(1)Cu), 3(x_{Au}(2)Au+x_{Cu}(2)Cu)]	*Pm*3*m*
Au_3Cu-type ordered alloy	Au(1)-rich sublattice, Cu(2) -rich sublattice	(x_{Au}(1)Au+x_{Cu}(1)Cu), (x_{Au}(2)Au+x_{Cu}(2)Cu)	[3(x_{Au}(1)Au+x_{Cu}(1)Cu), (x_{Au}(2)Au+x_{Cu}(2)Cu)]	*Pm*3*m*
Disordered alloy	FCC-basic lattice	(x_{Au}Au+x_{Cu}Cu)	[4(x_{Au}Au+x_{Cu}Cu)]	*Fm*3*m*

Table A.2 AGA-crystal structures of alloy phases in Au−Cu system

Phase	Basic lattice	Alloy gene at site	AGA-cell	Space group
Pure Au	FCC-lattice	A_0^{Au}	$[4A_0^{Au}]$	*Fm*3*m*
Pure Cu	FCC-lattice	A_{12}^{Cu}	$[4A_{12}^{Cu}]$	*Fm*3*m*
AuCu compounds	Au(1) sublattice, Cu(2) sublattice	$A_8^{Au}(1), A_4^{Cu}(2)$	$[2A_8^{Au}(1), 2A_4^{Cu}(2)]$	*P*4/*mmm*
$AuCu_3$ compounds	Au(1) sublattice, Cu(2) sublattice	$A_{12}^{Au}(1), A_8^{Cu}(2)$	$[A_{12}^{Au}(1), 3A_8^{Cu}(2)]$	*Pm*3*m*
Au_3Cu compounds	Au(1) sublattice, Cu(2) sublattice	$A_4^{Cu}(1), A_0^{Cu}(2)$	$[3A_4^{Au}(1), A_0^{Cu}(2)]$	*Pm*3*m*
AuCu-type ordered alloy	Au(1)-rich sublattice, Cu(2)-rich sublattice	$\sum(x_i^{Au}(1)/x_{Au}A_i^{Au}+x_i^{Cu}(1)/x_{Cu}A_i^{Cu})$, $\sum(x_i^{Au}(2)/x_{Au}A_i^{Au}+x_i^{Cu}(2)/x_{Cu}A_i^{Cu})$	$[2\sum(x_i^{Au}(1)/x_{Au}A_i^{Au}+x_i^{Cu}(1)/x_{Cu}A_i^{Cu}), 2\sum(x_i^{Au}(2)/x_{Au}A_i^{Au}+x_i^{Cu}(2)/x_{Cu}A_i^{Cu})]$	*P*4/*mmm*
$AuCu_3$-type ordered alloy	Au(1)-rich sublattice, Cu(2)-rich sublattice	$\sum(x_i^{Au}(1)/x_{Au}A_i^{Au}+x_i^{Cu}(1)/x_{Cu}A_i^{Cu})$, $\sum(x_i^{Au}(2)/x_{Au}A_i^{Au}+x_i^{Cu}(2)/x_{Cu}A_i^{Cu})$	$[\sum(x_i^{Au}(1)/x_{Au}A_i^{Au}+x_i^{Cu}(1)/x_{Cu}A_i^{Cu}), 3\sum(x_i^{Au}(2)/x_{Au}A_i^{Au}+x_i^{Cu}(2)/x_{Cu}A_i^{Cu})]$	*Pm*3*m*
Au_3Cu-type Ordered alloy	Au(1)-rich sublattice, Cu(2)-rich sublattice	$\sum(x_i^{Au}(1)/x_{Au}A_i^{Au}+x_i^{Cu}(1)/x_{Cu}A_i^{Cu})$, $\sum(x_i^{Au}(2)/x_{Au}A_i^{Au}+x_i^{Cu}(2)/x_{Cu}A_i^{Cu})$	$[3\sum(x_i^{Au}(1)/x_{Au}A_i^{Au}+x_i^{Cu}(1)/x_{Cu}A_i^{Cu}), \sum(x_i^{Au}(2)/x_{Au}A_i^{Au}+x_i^{Cu}(2)/x_{Cu}A_i^{Cu})]$	*Pm*3*m*
Disordered alloys	FCC-basic lattice	$\sum(x_i^{Au}A_i^{Au}+x_i^{Cu}A_i^{Cu})$	$4\sum(x_i^{Au}A_i^{Au}+x_i^{Cu}A_i^{Cu})$	*Fm*3*m*

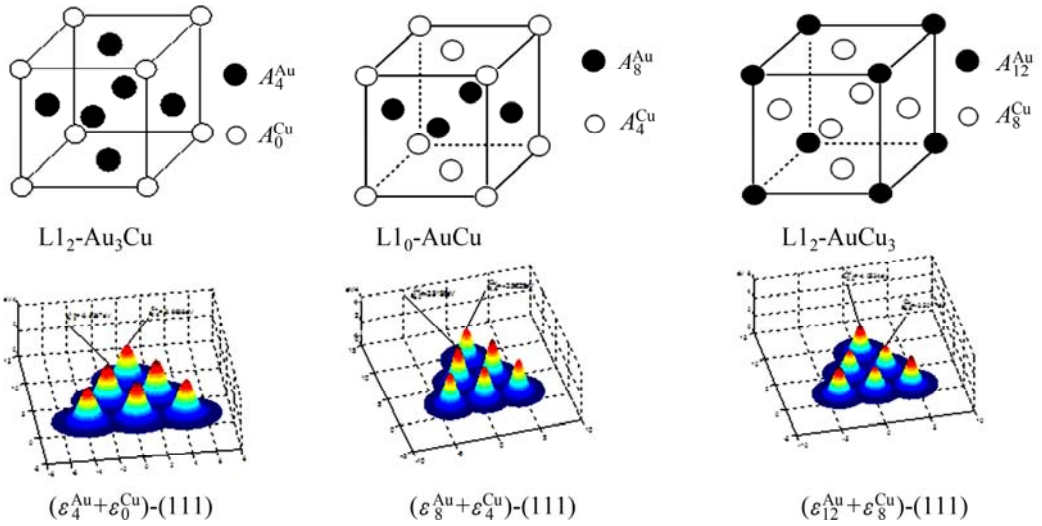

Fig. A.1 Characteristic atom arrangement cells and potential energy wave (111) planes of compounds $L1_2$-Au_3Cu, $L1_0$-AuCu and $L1_2$-$AuCu_3$

$$S_i^{\alpha.\mathrm{v}}(T)=S_i^{\alpha.\mathrm{D}}(T)+S_i^{\alpha.\mathrm{E}}(T) \tag{7}$$

$$U_i^{\alpha.\mathrm{D}}(T)=\int_0^T c_{pi}^{\alpha.\mathrm{D}}(T)\mathrm{d}T \tag{8}$$

$$U_i^{\alpha.\mathrm{E}}(T)=\int_0^T c_{pi}^{\alpha.\mathrm{E}}(T)\mathrm{d}T \tag{9}$$

$$S_i^{\alpha.\mathrm{D}}(T)=\int_0^T \frac{c_{pi}^{\alpha.\mathrm{D}}(T)}{T}\mathrm{d}T \tag{10}$$

$$S_i^{\alpha.\mathrm{E}}(T)=\int_0^T \frac{c_{pi}^{\alpha.\mathrm{E}}(T)}{T}\mathrm{d}T \tag{11}$$

$$\begin{cases}\theta_i^{Au}=\theta_0^{Au}\times\sqrt{E_i^{Au}(0)/(V_i^{Au}(0))^{(2/3)}}\,/\\ \quad\sqrt{E_0^{Au}(0)/(V_0^{Au}(0))^{(2/3)}}\\ \theta_i^{Cu}=\theta_I^{Cu}\times\sqrt{E_i^{Cu}(0)/(V_i^{Cu}(0))^{(2/3)}}\,/\\ \quad\sqrt{E_{12}^{Cu}(0)/(V_{12}^{Cu}(0))^{(2/3)}}\end{cases} \tag{12}$$

$$\begin{cases} c_{pi}^{\mathrm{Au.D}}(T)=9R\left(\dfrac{T}{\theta_i^{\mathrm{Au}}}\right)^3\int_0^{\theta_i^{\mathrm{Au}}/T}\dfrac{\mathrm{e}^x x^4}{(\mathrm{e}^x-1)^2}\mathrm{d}x \\ c_{pi}^{\mathrm{Cu.D}}(T)=9R\left(\dfrac{T}{\theta_i^{\mathrm{Cu}}}\right)^3\int_0^{\theta_i^{\mathrm{Cu}}/T}\dfrac{\mathrm{e}^x x^4}{(\mathrm{e}^x-1)^2}\mathrm{d}x \end{cases} \tag{13}$$

$$\begin{cases} c_{p0}^{\mathrm{Au.E}}(T)=1.858993\times10^{-10}T+4.222584\times10^{-6}T^2 \\ c_{p12}^{\mathrm{Au.E}}(T)=2.763134\times10^{-4}T+5.481502\times10^{-6}T^2 \end{cases} \tag{14}$$

$$\begin{cases} c_{p12}^{\mathrm{Cu.E}}(T)=0.00168035T+2.826912\times10^{-6}T^2 \\ c_{p0}^{\mathrm{Cu.E}}(T)=0.00564614T+3.632353\times10^{-6}T^2 \end{cases} \tag{15}$$

where α denotes Au or Cu; R is the gas constant; θ_0^{Au} =165 K, $\theta_{12}^{\mathrm{Au}}$ =175.21 K, $\theta_{12}^{\mathrm{Cu}}$ =343 K, θ_0^{Cu} =343.07 K.

It has been demonstrated that the q-energetic property sequence in the Au−Cu system may be described by following equation:

$$\begin{cases} q_i^{\mathrm{Au}}(T)=q_0^{\mathrm{Au}}(T)+(i/I)^2[q_I^{\mathrm{Au}}(T)-q_0^{\mathrm{Au}}(T)] \\ q_i^{\mathrm{Cu}}(T)=q_I^{\mathrm{Cu}}(T)+[(I-i)/I]^2[q_0^{\mathrm{Cu}}(T)-q_{\mathrm{I}}^{\mathrm{Cu}}(T)] \end{cases} \tag{16}$$

From Tables A.3 to A.6, therefore, it can be known that the so-called equilibrium order-disorder transition $E_{\min}$ - path obtained by the AGA-potential free energy function of the alloy is higher than the $G_{\min}$ - path obtained by the AGA-Gibbs free energy function, because the $G_i(T)$ is always lower than the corresponding $E_i(T)$; and the $T\times S_i^{\mathrm{v}}(T)$ is always larger than the corresponding $U_i(T)$.

A.3 Alloy gene Gibbs energy levels and alloy gene pair Gibbs energy levels

Analogous with AG-Gibbs energy partition function, the AG-pair Gibbs energy partition function may be used to describe systematic correlativity of the AG-pair Gibbs energy levels, the AG-cluster probabilities occupied at the AG-pair Gibbs energy levels and degeneracy function of these probabilities as function of composition (x), temperature (T) and order degree (σ), and to derive the Gibbs energy function.

In the Au−Cu system, the complete AG-pair sequences contain C_{26}^2=325 kinds of AG-pairs, which are $\sum_{i=0}^{12}\sum_{i'=0}^{12}(A_i^{\mathrm{Au}}-A_{i'}^{\mathrm{Au}})$, $\sum_{i=0}^{12}\sum_{i'=0}^{12}(A_i^{\mathrm{Cu}}-A_{i'}^{\mathrm{Cu}})$, $\sum_{i=0}^{12}\sum_{i'=0}^{12}(A_i^{\mathrm{Au}}-A_{i'}^{\mathrm{Cu}})$, and the complete AG-pair Gibbs energy sequences contain C_{26}^2=325 kinds of AG-pairs Gibbs energy levels, which are $\sum_{i=0}^{12}\sum_{i'=0}^{12}(G_i^{\mathrm{Au}}+G_{i'}^{\mathrm{Au}})$, $\sum_{i=0}^{12}\sum_{i'=0}^{12}(G_i^{\mathrm{Cu}}+G_{i'}^{\mathrm{Cu}})$, $\sum_{i=0}^{12}\sum_{i'=0}^{12}(G_i^{\mathrm{Au}}+G_{i'}^{\mathrm{Cu}})$. The AG-pair probabilities (i.e., concentrations) occupied at the AG-pair Gibbs energy levels are respectively $\sum_{i=0}^{12}\sum_{i'=0}^{12}\frac{1}{2}x_i^{\mathrm{Au}}x_{i'}^{\mathrm{Au}}$, $\sum_{i=0}^{12}\sum_{i'=0}^{12}\frac{1}{2}x_i^{\mathrm{Cu}}x_{i'}^{\mathrm{Cu}}$, $\sum_{i=0}^{12}\sum_{i'=0}^{12}x_i^{\mathrm{Au}}x_{i'}^{\mathrm{Cu}}$. Therefore, the AG-pair Gibbs energy partition function may be established and the characteristic Gibbs energy $G^*(x,T,\sigma)$ of an alloy should be

$$G^*(x,T,\sigma)=\sum_{i=0}^{12}\sum_{i'=0}^{12}[\frac{1}{2}x_i^{\mathrm{Au}}x_{i'}^{\mathrm{Au}}(G_i^{\mathrm{Au}}+G_{i'}^{\mathrm{Au}})+\frac{1}{2}x_i^{\mathrm{Cu}}x_{i'}^{\mathrm{Cu}}(G_i^{\mathrm{Cu}}+G_{i'}^{\mathrm{Cu}})+x_i^{\mathrm{Au}}x_{i'}^{\mathrm{Cu}}(G_i^{\mathrm{Au}}+G_{i'}^{\mathrm{Cu}})] \tag{17}$$

It may be proved that Eqs. (2) and (17) are equivalent. For the Au_3Cu ($(A_4^{\mathrm{Au}})_3A_0^{\mathrm{Cu}}$) compound with x_4^{Au}=75% Au and x_0^{Cu}=25% Cu, its molar characteristic Gibbs energy calculated by Eq. (17) is

$$G^*_{\mathrm{Au_3Cu}}(25\%\mathrm{Cu},T,1)=0.75G_4^{\mathrm{Au}}(T)+0.25G_0^{\mathrm{Cu}}(T)$$

For the AuCu($(A_8^{\mathrm{Au}}A_4^{\mathrm{Cu}})$) compound with x_8^{Au}= 50% Au and x_4^{Cu}=50% Cu, its molar characteristic Gibbs energy calculated by Eq. (17) is

$$G^*_{\mathrm{AuCu}}(50\%\mathrm{Cu},T,1)=0.5G_8^{\mathrm{Au}}(T)+0.5G_4^{\mathrm{Cu}}(T)$$

For the $AuCu_3$ $A_{12}^{\mathrm{Au}}(A_8^{\mathrm{Cu}})_3$ compound with x_{12}^{Au}= 25% Au and x_8^{Cu}=75% Cu, its molar characteristic Gibbs energy calculated by Eq. (17) is

$$G^*_{\mathrm{AuCu_3}}(75\%\mathrm{Cu},T,1)=0.25G_{12}^{\mathrm{Au}}(T)+0.75G_8^{\mathrm{Cu}}(T)$$

Analogous with AG-Gibbs energy partition function, the AG-cluster Gibbs energy partition function may be used to describe systematic correlativity of the AG-cluster Gibbs energy levels, the AG-cluster probabilities occupied at the AG-cluster Gibbs energy levels and degeneracy function of these probabilities as function of composition (x), temperature (T) and order degree (σ), and to derive the Gibbs energy function. However, for a given alloy, its characteristic Gibbs energies $G^*(x,T,\sigma)$, configuration entropy $S^{\mathrm{c}}(x,T,\sigma)$ and Gibbs energies $G(x,T,\sigma)$ calculated respectively by AG-, AG-pair and by AG-cluster sequence as structure unit sequences should be identical, because $G(x,T,\sigma)$, $G^*(x,T,\sigma)$ and $S^{\mathrm{c}}(x,T,\sigma)$ functions are interrelated. For simplified calculation, we should adopt AG-sequence as structure unit sequence, rather than AG-pair sequence and AG-cluster sequences. It has been also demonstrated that the configurational entropy is independent on sizes of structure units, if they are complete sequences.

A.4 Configurational entropy and configurational entropy energy

In the SMMS-framework, the AG-Gibbs energy function derived from the AG-Gibbs energy partition function in the Au−Cu system is a complex function with multi-levels:

Table A.3 E_0^{Au}, $U_0^{Au.v}$, c_{p0}^{Au}, $H_0^{Au.v}$, $(T\times S_0^{Au.v})$, G_0^{Au}, $\left|E_0^{Au}/U_0^{Au.v}\right|$ and $(T\times S_0^{Au.v}-U_0^{Au.v})$ of A_0^{Au}-alloy gene

T/K	E_0^{Au}/ (J·mol^{-1})	$U_0^{Au.v}$ ①/ (J·mol^{-1})	c_{p0}^{Au}/ (J·mol^{-1}·K^{-1})	$H_0^{Au.v}$/ (J·mol^{-1})	$(T\times S_0^{Au.v})$/ (J·mol^{-1})	G_0^{Au}/ (J·mol^{-1})	$\left\|E_0^{Au}/U_0^{Au.v}\right\|$	$(T\times S_0^{Au.v}-U_0^{Au.v})$/ (J·mol^{-1})
0	−368000	0	0.00	−368000	0	−368000	−	0
50	−368000	310	15.30	−367690	460	−368150	1188.84	150
100	−368000	1281	21.89	−366719	2241	−368959	287.19	960
150	−368000	2426	23.59	−365574	4750	−370324	151.69	2324
200	−368000	3625	24.28	−364375	7712	−372087	101.52	4087
250	−368000	4849	24.67	−363151	11005	−374156	75.89	6156
300	−368000	6090	24.95	−361910	14563	−376473	60.43	8473
350	−368000	7344	25.18	−360656	18343	−379000	50.11	10999
400	−368000	8608	25.41	−359392	22314	−381706	42.75	13706
450	−368000	9884	25.63	−358116	26456	−384572	37.23	16572
500	−368000	11171	25.86	−356829	30752	−387580	32.94	19581
550	−368000	12471	26.11	−355529	35189	−390718	29.51	22718
593	−368000	13598	26.33	−354402	39111	−393512	27.06	25513
600	−368000	13782	26.37	−354218	39758	−393975	26.70	25976
620	−368000	14311	26.48	−353689	41620	−395309	25.71	27309
637	−368000	14762	26.57	−353238	43218	−396457	24.93	28456
650	−368000	15108	26.65	−352892	44450	−397342	24.36	29342
683	−368000	15990	26.84	−352010	47611	−399621	23.01	31621
700	−368000	16447	26.94	−351553	49259	−400811	22.37	32812
750	−368000	17802	27.26	−350198	54179	−404377	20.67	36377
769	−368000	18321	27.38	−349679	56077	−405756	20.09	37756
800	−368000	19173	27.59	−348827	59207	−408034	19.19	40034
850	−368000	20562	27.95	−347438	64338	−411777	17.90	43776
900	−368000	21968	28.32	−346032	69570	−415602	16.75	47602
950	−368000	23394	28.72	−344606	74900	−419505	15.73	51506
1000	−368000	24840	29.13	−343160	80325	−423485	14.81	55485
1050	−368000	26308	29.57	−341692	85845	−427537	13.99	59537
1100	−368000	27797	30.02	−340203	91457	−431660	13.24	63660
1150	−368000	29310	30.50	−338690	97161	−435851	12.56	67851
1200	−368000	30848	31.00	−337152	102955	−440108	11.93	72107
1250	−368000	32410	31.52	−335590	108840	−444430	11.35	76430
1300	−368000	34000	32.06	−334000	114814	−448815	10.82	80814
1336②	−368000	35161	32.46	−332839	119171	−452010	10.47	84010
1350	−368000	35617	32.62	−332383	120878	−453261	10.33	85261
1356③	−368000	35813	32.69	−332187	121611	−453799	10.28	85798
1400	−368000	37262	33.20	−330738	127030	−457768	9.88	89768

① The generalized vibration energy includes contributions of Debye vibration energy, existing energy of electrons, forming energy of holes, expansion work of volume and variation in potential energy with temperature; ② The melting of pure Au metal; ③ The melting of pure Cu metal.

Table A.4 E_{12}^{Cu}, $U_{12}^{Cu.v}$, c_{p12}^{Cu}, $H_{12}^{Cu,v}$, $(T\times S_{12}^{Cu,v})$, G_{12}^{Cu}, $\left|E_{12}^{Cu}/U_{12}^{Cu,v}\right|$ and $(T\times S_{12}^{Cu,v}-U_{12}^{Cu,v})$ of A_{12}^{Cu}-alloy gene

T/K	E_{12}^{Cu} / (J·mol^{-1})	$U_{12}^{Cu.v}$ ① / (J·mol^{-1})	c_{p12}^{Cu} / (J·mol^{-1}·K^{-1})	$H_{12}^{Cu,v}$ / (J·mol^{-1})	$(T\times S_{12}^{Cu,v})$ / (J·mol^{-1})	G_{12}^{Cu} / (J·mol^{-1})	$\left\|E_{12}^{Cu}/U_{12}^{Cu,v}\right\|$	$(T\times S_{12}^{Cu,v}-U_{12}^{Cu,v})$ / (J·mol^{-1})
0	−336000	0	0.00	−336000	0	−336000	−	0
50	−336000	71	5.08	−335929	98	−336026	4715.07	27
100	−336000	593	14.96	−335407	879	−336286	566.38	286
150	−336000	1478	19.78	−334522	2384	−336907	227.37	906
200	−336000	2531	22.08	−333469	4387	−337857	132.77	1856
250	−336000	3669	23.34	−332331	6753	−339084	91.58	3084
300	−336000	4857	24.14	−331143	9403	−340546	69.18	4546
350	−336000	6079	24.72	−329921	12288	−342209	55.27	6209
400	−336000	7327	25.17	−328673	15376	−344049	45.86	8049
450	−336000	8596	25.56	−327404	18643	−346047	39.09	10047
500	−336000	9882	25.91	−326118	22070	−348188	34.00	12188
550	−336000	11186	26.24	−324814	25644	−350458	30.04	14458
593	−336000	12321	26.52	−323679	28826	−352506	27.27	16505
600	−336000	12507	26.57	−323493	29354	−352847	26.87	16847
620	−336000	13039	26.69	−322961	30873	−353834	25.77	17834
637	−336000	13494	26.80	−322506	32181	−354687	24.90	18687
650	−336000	13843	26.88	−322157	33190	−355347	24.27	19347
683	−336000	14734	27.10	−321266	35788	−357054	22.81	21054
700	−336000	15195	27.21	−320805	37146	−357951	22.11	21951
750	−336000	16564	27.53	−319436	41215	−360652	20.29	24651
769	−336000	17088	27.66	−318912	42790	−361703	19.66	25702
800	−336000	17949	27.87	−318051	45393	−363445	18.72	27444
850	−336000	19351	28.21	−316649	49675	−366324	17.36	30324
900	−336000	20770	28.56	−315230	54057	−369287	16.18	33287
950	−336000	22207	28.93	−313793	58537	−372330	15.13	36330
1000	−336000	23663	29.30	−312337	63111	−375448	14.20	39448
1050	−336000	25138	29.69	−310862	67778	−378640	13.37	42640
1100	−336000	26632	30.09	−309368	72534	−381902	12.62	45902
1150	−336000	28147	30.50	−307853	77380	−385233	11.94	49233
1200	−336000	29683	30.93	−306317	82313	−388630	11.32	52630
1250	−336000	31240	31.37	−304760	87332	−392092	10.76	56092
1300	−336000	32819	31.82	−303181	92436	−395616	10.24	59617
1336②	−336000	33971	32.15	−302029	96163	−398192	9.89	62192
1350	−336000	34422	32.28	−301578	97624	−399202	9.76	63202
1356③	−336000	34616	32.34	−301384	98252	−399636	9.71	63636
1400	−336000	36048	32.76	−299952	102895	−402847	9.32	66847

① The generalized vibration energy includes contributions of Debye vibration energy, existing energy of electrons, forming energy of holes, expansion work of volume and variation in potential energy with temperature; ② The melting of pure Au metal; ③ The melting of pure Cu metal.

Table A.5 E_{12}^{Au}, $U_{12}^{Au.v}$, c_{p12}^{Au}, $H_{12}^{Au.v}$, $(T\times S_{12}^{Au.v})$, G_{12}^{Au}, $\left|E_{12}^{Au}/U_{12}^{Au.v}\right|$ and $(T\times S_{12}^{Au.v}-U_{12}^{Au.v})$ of A_{12}^{Au}-alloy gene

T/K	E_{12}^{Au} / (J·mol^{-1})	$U_{12}^{Au.v}$ ① / (J·mol^{-1})	c_{p12}^{Au} / (J·mol^{-1}·K^{-1})	$H_{12}^{Au.v}$ / (J·mol^{-1})	$(T\times S_{12}^{Au.v})$ / (J·mol^{-1})	G_{12}^{Au} / (J·mol^{-1})	$\left\|E_{12}^{Au}/U_{12}^{Au.v}\right\|$	$(T\times S_{12}^{Au.v}-U_{12}^{Au.v})$ / (J·mol^{-1})
0	−391303	0	0.00	−391303	0	−391303	−	0
50	−391303	283	14.49	−391020	416	−391435	1382.57	133
100	−391303	1228	21.58	−390074	2114	−392188	318.59	886
150	−391303	2363	23.48	−388940	4547	−393487	165.60	2184
200	−391303	3559	24.29	−387743	7439	−395182	109.93	3880
250	−391303	4786	24.75	−386517	10667	−397183	81.76	5881
300	−391303	6033	25.10	−385270	14163	−399433	64.86	8130
350	−391303	7295	25.40	−384007	17886	−401893	53.64	10591
400	−391303	8573	25.69	−382730	21805	−404535	45.65	13232
450	−391303	9865	25.99	−381438	25900	−407339	39.67	16035
500	−391303	11172	26.30	−380131	30155	−410286	35.03	18983
550	−391303	12495	26.63	−378808	34558	−413366	31.32	22063
593	−391303	13646	26.92	−377657	38455	−416111	28.68	24809
600	−391303	13835	26.98	−377468	39098	−416566	28.28	25263
620	−391303	14376	27.12	−376927	40951	−417879	27.22	26575
637	−391303	14838	27.25	−376465	42543	−419008	26.37	27705
650	−391303	15193	27.35	−376110	43769	−419879	25.76	28576
683	−391303	16099	27.61	−375203	46921	−422124	24.31	30822
700	−391303	16570	27.74	−374733	48565	−423298	23.62	31995
750	−391303	17967	28.16	−373335	53480	−426815	21.78	35513
769	−391303	18504	28.33	−372799	55378	−428177	21.15	36874
800	−391303	19387	28.61	−371916	58511	−430427	20.18	39124
850	−391303	20829	29.08	−370474	63654	−434128	18.79	42825
900	−391303	22295	29.58	−369007	68907	−437914	17.55	46612
950	−391303	23788	30.11	−367515	74268	−441783	16.45	50480
1000	−391303	25307	30.66	−365996	79735	−445731	15.46	54428
1050	−391303	26854	31.24	−364448	85307	−449756	14.57	58453
1100	−391303	28431	31.85	−362871	90984	−453855	13.76	62553
1150	−391303	30039	32.48	−361263	96763	−458027	13.03	66724
1200	−391303	31680	33.14	−359623	102646	−462269	12.35	70966
1250	−391303	33354	33.83	−357949	108631	−466580	11.73	75277
1300	−391303	35063	34.54	−356240	114719	−470959	11.16	79656
1336②	−391303	36316	35.07	−354987	119166	−474153	10.77	82850
1350	−391303	36809	35.28	−354494	120910	−475404	10.63	84101
1356③	−391303	37021	35.37	−354282	121660	−475942	10.57	84639
1400	−391303	38592	36.05	−352711	127204	−479915	10.14	88612

① The generalized vibration energy includes contributions of Debye vibration energy, existing energy of electrons, forming energy of holes, expansion work of volume and variation in potential energy with temperature; ② The melting of pure Au metal; ③ The melting of pure Cu metal.

Table A.6 E_0^{Cu}, $U_0^{Cu.v}$, c_{p0}^{Cu}, $H_0^{Cu.v}$, $(T\times S_0^{Cu.v})$, G_0^{Cu}, $\left|E_0^{Cu}/U_0^{Cu.v}\right|$ and $(T\times S_0^{Cu.v}-U_0^{Cu.v})$ of the A_0^{Cu}-alloy gene

T/K	E_0^{Cu} / (J·mol^{-1})	$U_0^{Cu.v}$ ① / (J·mol^{-1})	c_{p0}^{Cu} / (J·mol^{-1}·K^{-1})	$H_0^{Cu.v}$ / (J·mol^{-1})	$(T\times S_0^{Cu.v})$ / (J·mol^{-1})	G_0^{Cu} / (J·mol^{-1})	$\left\|E_0^{Cu}/U_0^{Cu.v}\right\|$	$(T\times S_0^{Cu.v}-U_0^{Cu.v})$ / (J·mol^{-1})
0	−352055	0	0.00	−352055	0	−352055	−	0
50	−352055	76	5.27	−351979	108	−352087	4619.24	32
100	−352055	613	15.36	−351442	918	−352361	574.17	305
150	−352055	1523	20.39	−350532	2474	−353006	231.16	951
200	−352055	2612	22.90	−349444	4548	−353992	134.80	1936
250	−352055	3796	24.38	−348259	7005	−355264	92.73	3209
300	−352055	5042	25.41	−347013	9769	−356782	69.82	4727
350	−352055	6333	26.20	−345722	12789	−358511	55.59	6456
400	−352055	7661	26.89	−344394	16034	−360428	45.95	8373
450	−352055	9021	27.51	−343034	19480	−362514	39.03	10459
500	−352055	10411	28.10	−341644	23109	−364753	33.81	12698
550	−352055	11830	28.67	−340225	26907	−367132	29.76	15077
593	−352055	13074	29.16	−338982	30301	−369283	26.93	17227
600	−352055	13278	29.23	−338777	30864	−369642	26.51	17586
620	−352055	13865	29.46	−338190	32490	−370680	25.39	18625
637	−352055	14367	29.65	−337688	33890	−371578	24.50	19523
650	−352055	14754	29.80	−337302	34972	−372274	23.86	20218
683	−352055	15744	30.18	−336312	37762	−374074	22.36	22018
700	−352055	16258	30.38	−335797	39223	−375020	21.65	22965
750	−352055	17792	30.96	−334264	43611	−377875	19.79	25819
769	−352055	18382	31.19	−333673	45314	−378987	19.15	26932
800	−352055	19355	31.56	−332701	48132	−380833	18.19	28777
850	−352055	20947	32.16	−331108	52782	−383890	16.81	31835
900	−352055	22571	32.79	−329484	57557	−387042	15.60	34986
950	−352055	24226	33.42	−327829	62455	−390284	14.53	38229
1000	−352055	25914	34.07	−326142	67473	−393615	13.59	41559
1050	−352055	27634	34.74	−324421	72609	−397031	12.74	44975
1100	−352055	29388	35.43	−322667	77862	−400529	11.98	48474
1150	−352055	31177	36.13	−320878	83230	−404108	11.29	52053
1200	−352055	33001	36.85	−319054	88712	−407766	10.67	55711
1250	−352055	34862	37.58	−317193	94307	−411500	10.10	59445
1300	−352055	36760	38.33	−315296	100014	−415310	9.58	63254
1336②	−352055	38150	38.89	−313906	104193	−418099	9.23	66043
1350	−352055	38696	39.10	−313360	105834	−419193	9.10	67138
1356③	−352055	38930	39.20	−313125	106539	−419664	9.04	67609
1400	−352055	40670	39.89	−311385	111764	−423149	8.66	71094

① The generalized vibration energy includes contributions of Debye vibration energy, existing energy of electrons, forming energy of holes, expansion work of volume and variation in potential energy with temperature; ② The melting of pure Au metal; ③ The melting of pure Cu metal.

$$\begin{cases} G(x,T,\sigma)=G^{*}(x,T,\sigma)-TS^{\mathrm{c}}(x,T,\sigma), \\ G^{*}(x,T,\sigma)=E(x,T,\sigma)+U^{\mathrm{v}}(x,T,\sigma)-TS^{\mathrm{v}}(x,T,\sigma), \\ H(x,T,\sigma)=E(x,T,\sigma)+U^{\mathrm{v}}(x,T,\sigma), \\ E(x,T,\sigma)=\sum_{i=0}^{12}[x_i^{\mathrm{Au}}(x,T,\sigma)E_i^{\mathrm{Au}}(0)+ \\ \qquad x_i^{\mathrm{Cu}}(x,T,\sigma)E_i^{\mathrm{Cu}}(0)], \\ U^{\mathrm{v}}(x,T,\sigma)=\sum_{i=0}^{12}[x_i^{\mathrm{Au}}(x,T,\sigma)U_i^{\mathrm{Au.v}}(T)+ \\ \qquad x_i^{\mathrm{Cu}}(x,T,\sigma)U_i^{\mathrm{Cu.v}}(T)], \\ S^{\mathrm{v}}(x,T,\sigma)=\sum_{i=0}^{12}[x_i^{\mathrm{Au}}(x,T,\sigma)S_i^{\mathrm{Au.v}}(T)+ \\ \qquad x_i^{\mathrm{Cu}}(x,T,\sigma)S_i^{\mathrm{Cu.v}}(T)], \\ TS^{\mathrm{v}}(x,T,\sigma)=T\times\sum_{i=0}^{12}[x_i^{\mathrm{Au}}(x,T,\sigma)S_i^{\mathrm{Au.v}}(T)+ \\ \qquad x_i^{\mathrm{Cu}}(x,T,\sigma)S_i^{\mathrm{Cu.v}}(T)], \\ S^{\mathrm{c}}(x,T,\sigma)=k_{\mathrm{B}}\ln[g(x_i^{\mathrm{Au}}(x,T,\sigma),x_i^{\mathrm{Cu}}(x,T,\sigma)], \\ TS^{\mathrm{c}}(x,T,\sigma)=T\times k_{\mathrm{B}}\ln[g(x_i^{\mathrm{Au}}(x,T,\sigma),x_i^{\mathrm{Cu}}(x,T,\sigma)] \end{cases} \tag{18}$$

The following understandings have been obtained:

1) Once the AG-holographic information database of the fcc lattice based Au−Cu system has been established, the AG-$G(x,T,\sigma)$ function can be used to described the ordered alloys in the Au_3Cu-, AuCu- and $AuCu_3$-type sublattice systems and disordered alloy, where there is no unknown parameter.

2) The AG-propabilities $(x_i^{\mathrm{Au}},x_i^{\mathrm{Cu}})$ occupied at the AG-Gibbs energy levels of the equilibrium order−disorder transition for a given alloy are determined by the minimum mixed Gibbs energy $\Delta G_{\min}^{\mathrm{m}}-T$ path method [1].

3) The AG-propabilities $(x_i^{\mathrm{Au}},x_i^{\mathrm{Cu}})$ occupied at the AG-Gibbs energy levels of the subequilibrium order−disorder transition for a given alloy are determined by the experimental mixed enthalpy $\Delta H_{\exp}^{\mathrm{m}}-T$ tracking path method [16].

4) The $G^{*}(x,T,\sigma)$, $H(x,T,\sigma)$, $E(x,T,\sigma)$, $U^{\mathrm{v}}(x,T,\sigma)$, $S^{\mathrm{v}}(x,T,\sigma)$ and $S^{\mathrm{c}}(x,T,\sigma)$ functions are internected. It means that the configurational entropy $S^{\mathrm{c}}(x,T,\sigma)$ function can not be independently treated.

5) According to the first rule, it has been known that the constituent atoms, constituent atom pairs and constituent atom clusters can not be used as structure unit sequences, because they are incomplete sequences and have no their Gibbs energy levels.

6) According to the second rule, it has been known that the established so-called Gibbs energy functions with a number of unknown parameters by the constituent atoms, constituent atom pairs and constituent atom clusters are too crude in theory, and that based on the miss understandings of experimental information, these parameters are adjusted until the Gibbs energy function is capable of representing the experimental information, which is also questionable in practice.

7) According to the third and fourth rules, it has been known that if using AG-pairs with AG-pairs Gibbs energy levels and AG-clusters with AG-cluster Gibbs energy levels as structure units sequences, the calculated total Gibbs energies, characteristic Gibbs energies, potential energies, generalized vibration energies, generalized vibration entropies and configurational entropies are still identical respectively with ones obtained by the AG-sequences. It means that the configurational entropy is independent on sizes of structure units.

In order to understand how to calculate the configurational entropy from the AG-propabilities $(x_i^{\mathrm{Au}},x_i^{\mathrm{Cu}})$ occupied at the AG-Gibbs energy levels, we have calculated the $S^{\mathrm{c}}(x,T,\sigma)$ EHNP-diagrams of the Au_3Cu-, AuCu-, $AuCu_3$-type sublattice systems by Eqs. (19)−(24), which are shown in Figs. A.2−A.5. In our opinion, the AG-propabilities occupied at the AG-Gibbs energy levels in the degeneracy *g*-function should be degenerated by the ones of the constituent atoms occupied at the lattice points, based on following reasons:

1) The generalized vibration entropy $S^{\mathrm{v}}(x,T,\sigma)$ has been accounted in the $G^{*}(x,T,\sigma)$ -characteristic Gibbs energy (see Eq. (18)). Therefore, the configurational entropy $S^{\mathrm{c}}(x,T,\sigma)$, arisen from the AG-propabilities occupied at the lattice points should be degenerated by ones of the constituent atoms occupied at the lattice points.

2) The configurational entropy of each ordered alloy calculated by a degeneracy function can change continually from the configurational entropy in the maximum order degree state to one in the perfectly disordered state.

3) For binary alloy systems, the $S^{\mathrm{c}}(x,T,\sigma)$ should lie in the range:

$$0\leq S^{\mathrm{c}}(x,T,\sigma)\leq 5.763\ (\mathrm{J\cdot mol^{-1}\cdot K^{-1}})$$

where the upper limit is the value for a perfectly disordered equiatomic alloy.

The results show that the AGA-degeneracy function (1) and entropy function (1) may be used. The calculated details may be seen in Refs. [1,40,41].

The AGA degeneracy function (1) and entropy function (1):

$$g(x,T,\sigma)^{(1)}=\frac{\left[N\sum_{i=0}^{I}(x_i^{\mathrm{Au}(1)}+x_i^{\mathrm{Cu}(1)})\right]!}{\left(\sum_{i=0}^{I}Nx_i^{\mathrm{Au}(1)}\right)!\left(\sum_{i=0}^{I}Nx_i^{\mathrm{Cu}(1)}\right)!}\times$$

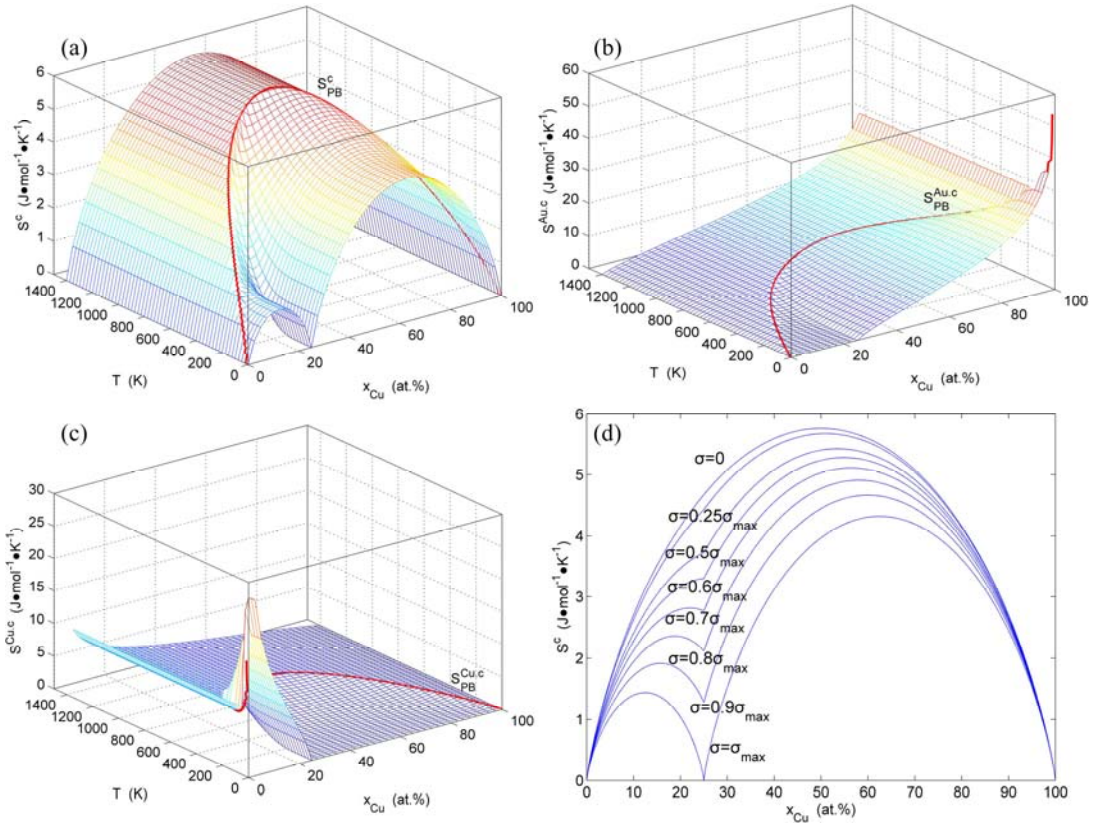

Fig. A.2 Configuration entropy EHNP diagrams of Au_3Cu-type sublattice system systems calculated by $S^{c}(x,T,\sigma)^{(1)}$-function: (a) Three-dimensional $S^{c}-x-T$ phase diagram with phase boundary curve $S^{c}_{PB}(x,T)$; (b) Three-dimensional $S^{c.Au}-x-T$ phase diagram with phase boundary curve $S^{c.Au}_{PB}(x,T)$ of Au-component; (c) Three-dimensional $S^{c.Cu}-x-T$ diagram with phase boundary curve $S^{c.Cu}_{PB}(x,T)$ of Cu-component; (d) $S^{c}(x,\sigma)$ curves at different σ values as function of $\sigma_{max}(x)$

$$\frac{\left[N\sum_{i=0}^{I}(x_i^{\mathrm{Au}(2)}+x_i^{\mathrm{Cu}(2)})\right]!}{\left(\sum_{i=0}^{I}Nx_i^{\mathrm{Au}(2)}\right)!\left(\sum_{i=0}^{I}Nx_i^{\mathrm{Cu}(2)}\right)!} \tag{19}$$

$$S^{c}(x,T,\sigma)^{(1)}=k_{\mathrm{B}}\ln\frac{\left[N\sum_{i=0}^{I}(x_i^{\mathrm{Au}(1)}+x_i^{\mathrm{Cu}(1)})\right]!}{\left(\sum_{i=0}^{I}Nx_i^{\mathrm{Au}(1)}\right)!\left(\sum_{i=0}^{I}Nx_i^{\mathrm{Cu}(1)}\right)!}\times$$

$$\frac{\left[N\sum_{i=0}^{I}(x_i^{\mathrm{Au}(2)}+x_i^{\mathrm{Cu}(2)})\right]!}{\left(\sum_{i=0}^{I}Nx_i^{\mathrm{Au}(2)}\right)!\left(\sum_{i=0}^{I}Nx_i^{\mathrm{Cu}(2)}\right)!} \tag{20}$$

The AGA degeneracy function (2) and entropy function (2):

$$g(x,T,\sigma)^{(2)}=\frac{\left[N\sum_{i=0}^{I}x_i^{\mathrm{Au}(1)}\right]!\left[\sum_{i=0}^{I}Nx_i^{\mathrm{Cu}(1)}\right]!}{\left(\prod_{i=0}^{I}Nx_i^{\mathrm{Au}(1)}\right)!\left(\prod_{i=0}^{I}Nx_i^{\mathrm{Cu}(1)}\right)!}\times$$

$$\frac{\left[N\sum_{i=0}^{I}x_i^{\mathrm{Au}(2)}\right]!\left[\sum_{i=0}^{I}Nx_i^{\mathrm{Cu}(2)}\right]!}{\left(\prod_{i=0}^{I}Nx_i^{\mathrm{Au}(2)}\right)!\left(\prod_{i=0}^{I}Nx_i^{\mathrm{Cu}(2)}\right)!} \tag{21}$$

$$S^{c}(x,T,\sigma)^{(2)}=k_{\mathrm{B}}\ln\frac{\left[N\sum_{i=0}^{I}x_i^{\mathrm{Au}(1)}\right]!\left[\sum_{i=0}^{I}Nx_i^{\mathrm{Cu}(1)}\right]!}{\left(\prod_{i=0}^{I}Nx_i^{\mathrm{Au}(1)}\right)!\left(\prod_{i=0}^{I}Nx_i^{\mathrm{Cu}(1)}\right)!}\times$$

$$\frac{\left[N\sum_{i=0}^{I}x_i^{\mathrm{Au}(2)}\right]!\left[\sum_{i=0}^{I}Nx_i^{\mathrm{Cu}(2)}\right]!}{\left(\prod_{i=0}^{I}Nx_i^{\mathrm{Au}(2)}\right)!\left(\prod_{i=0}^{I}Nx_i^{\mathrm{Cu}(2)}\right)!} \tag{22}$$

The AGA degeneracy function (3) and entropy function (3):

$$g(x,T,\sigma)^{(3)}=\frac{\left[N\sum_{i=0}^{I}(x_i^{\mathrm{Au}(1)}+x_i^{\mathrm{Cu}(1)})\right]!}{\left(\prod_{i=0}^{I}Nx_i^{\mathrm{Au}(1)}\right)!\left(\prod_{i=0}^{I}Nx_i^{\mathrm{Cu}(1)}\right)!}\times$$

$$\frac{\left[N\sum_{i=0}^{I}(x_i^{\mathrm{Au}(2)}+x_i^{\mathrm{Cu}(2)})\right]!}{\left(\prod_{i=0}^{I}Nx_i^{\mathrm{Au}(2)}\right)!\left(\prod_{i=0}^{I}Nx_i^{\mathrm{Cu}(2)}\right)!} \tag{23}$$

$$S^{\mathrm{c}}(x,T,\sigma)^{(3)}=k_{\mathrm{B}}\ln\frac{\left[N\sum_{i=0}^{I}(x_i^{\mathrm{Au}(1)}+x_i^{\mathrm{Cu}(1)})\right]!}{\left(\prod_{i=0}^{I}Nx_i^{\mathrm{Au}(1)}\right)!\left(\prod_{i=0}^{I}Nx_i^{\mathrm{Cu}(1)}\right)!}\times$$

$$\frac{\left[N\sum_{i=0}^{I}(x_i^{\mathrm{Au}(2)}+x_i^{\mathrm{Cu}(2)})\right]!}{\left(\prod_{i=0}^{I}Nx_i^{\mathrm{Au}(2)}\right)!\left(\prod_{i=0}^{I}Nx_i^{\mathrm{Cu}(2)}\right)!} \tag{24}$$

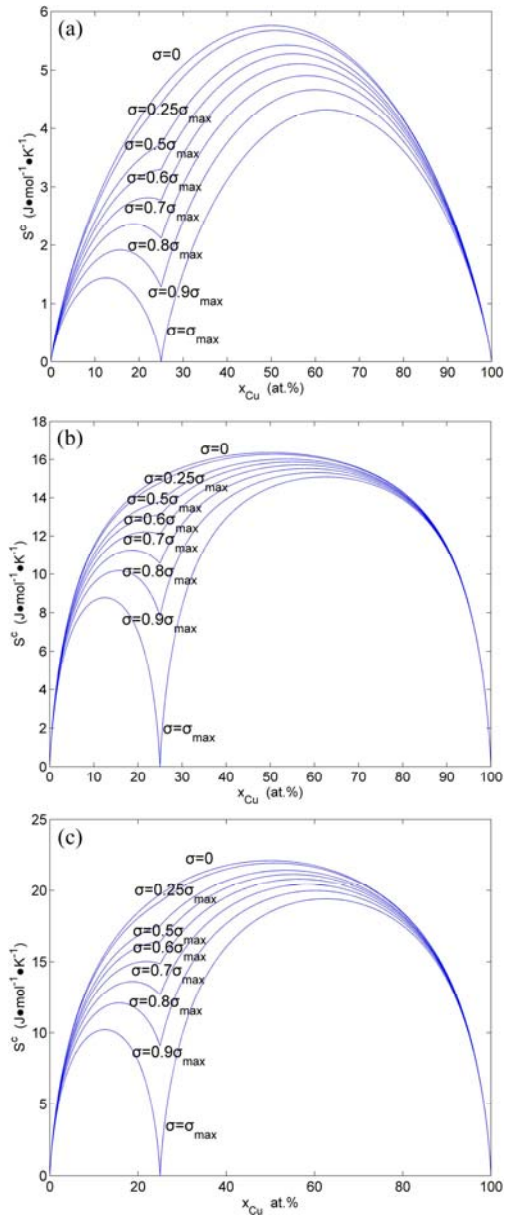

Fig. A.3 Congfiguration entropies of Au_3Cu-type sublattice system: (a) Calculated by $S^{\mathrm{c}}(x,T,\sigma)^{(1)}$; (b) Calculated by $S^{\mathrm{c}}(x,T,\sigma)^{(2)}$; (c) Calculated by $S^{\mathrm{c}}(x,T,\sigma)^{(3)}$

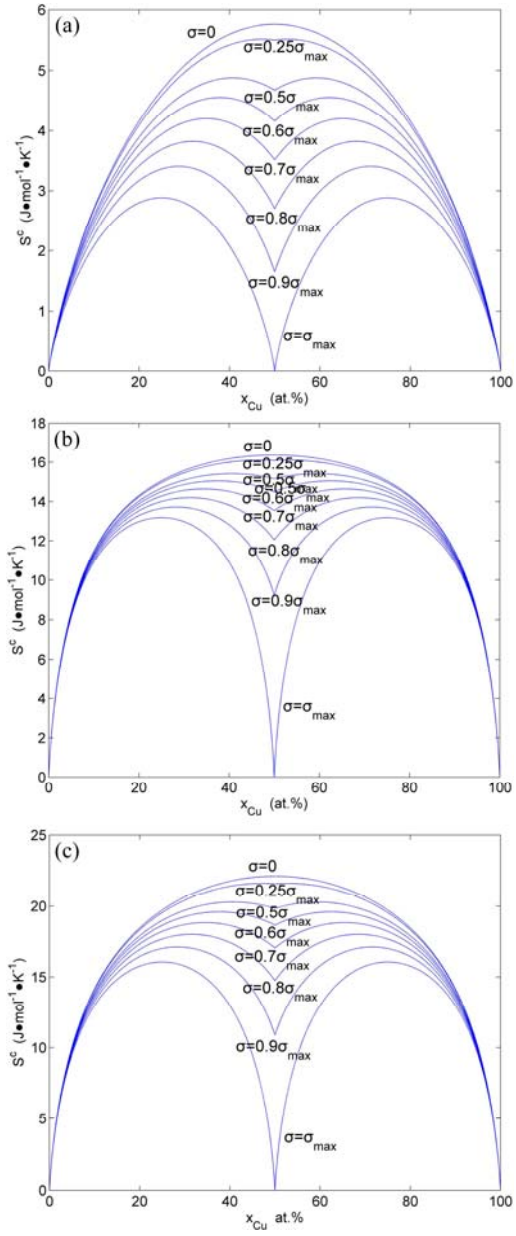

Fig. A.4 Congfiguration entropies of AuCu-type sublattice system: (a) Calculated by $S^{\mathrm{c}}(x,T,\sigma)^{(1)}$; (b) Calculated by $S^{\mathrm{c}}(x,T,\sigma)^{(2)}$; (c) Calculated by $S^{\mathrm{c}}(x,T,\sigma)^{(3)}$

B EHNP-charts on disordering stoichiometric Au_3Cu compound

According to $x_{i,\mathrm{e}}^{\mathrm{Au}}-T$ and $x_{i,\mathrm{e}}^{\mathrm{Cu}}-T$ paths on disordering stoichiometric Au_3Cu compound obtained by the minimal mixed Gibbs energy $\Delta G_{\min}^{\mathrm{m}}-T$ method, the EHNP charts are calculated and shown in Figs. B.1 to B.13. By the same method, the systematic correlativity data of the $\Delta G_{\mathrm{e}}^{\mathrm{m}}(x,T)$, $\sigma_{\mathrm{e}}(x,T)$, $S^{\mathrm{c}}(x,T)$, $x_{i,\mathrm{e}}^{\mathrm{Au}}(x,T)$ and $x_{i,\mathrm{e}}^{\mathrm{Cu}}(x,T)$ on equilibrium order-disorder transition paths as function of composition and temperature for alloys of the Au_3Cu-type sublattice system are calculated, using calculated steps Δx =0.5%, ΔT =1 K, $\Delta\sigma$ = 0.0001.

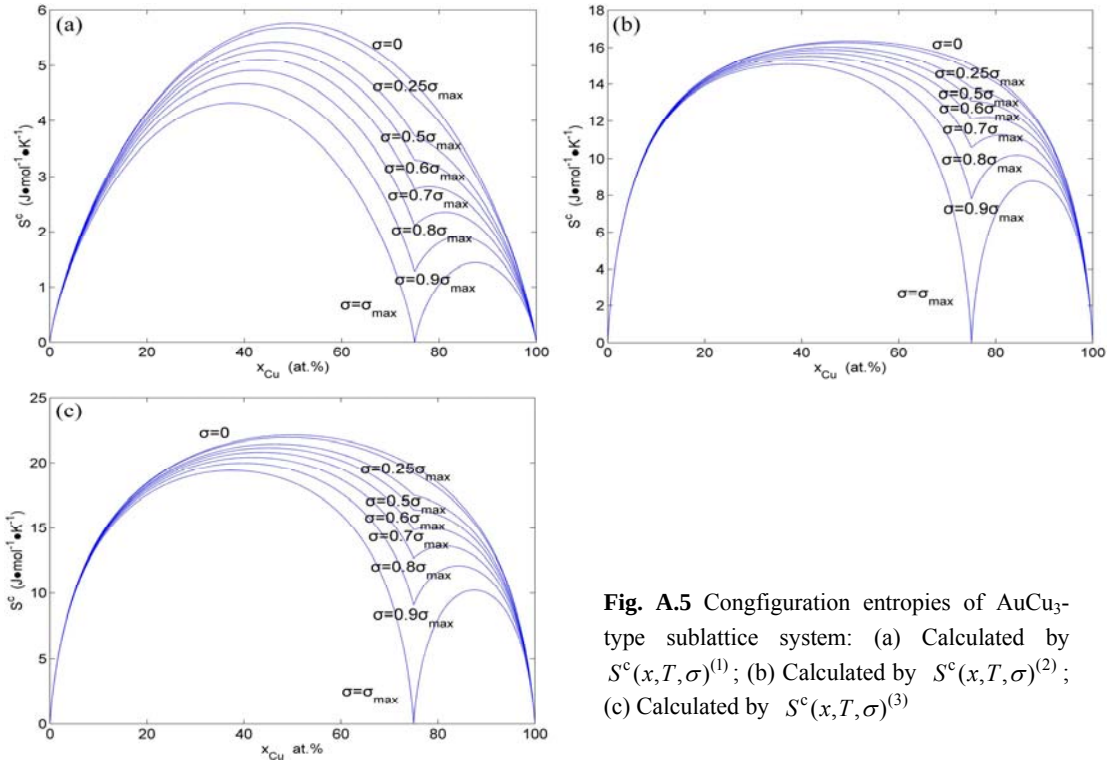

Fig. A.5 Congfiguration entropies of $AuCu_3$-type sublattice system: (a) Calculated by $S^{c}(x,T,\sigma)^{(1)}$; (b) Calculated by $S^{c}(x,T,\sigma)^{(2)}$; (c) Calculated by $S^{c}(x,T,\sigma)^{(3)}$

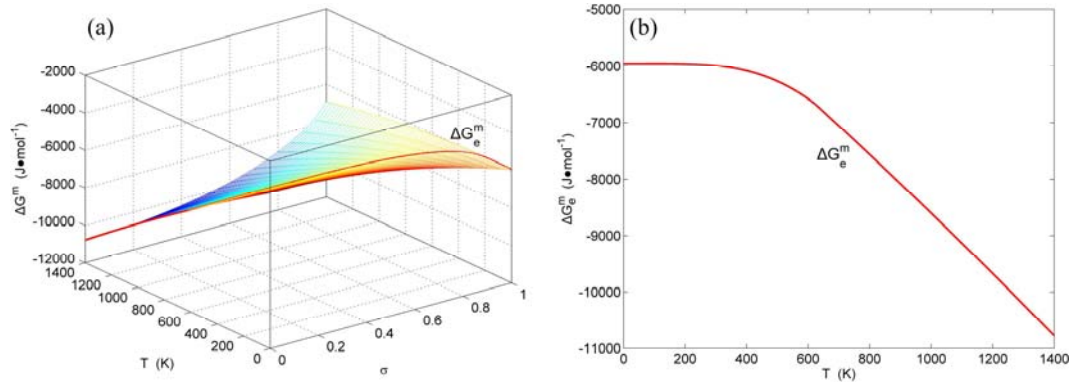

Fig. B.1 EHNP charts with EHNP curve of first order thermodynamic properties on disordering $Au_3Cu((A_4^{Au})_3A_0^{Cu})$: (a) Three-dimensional mixed Gibbs energy $\Delta G^{m}-T-\sigma$ EHNP chart with $\Delta G_{e}^{m}-T$ paths; (b) $\Delta G_{e}^{m}-T$ path

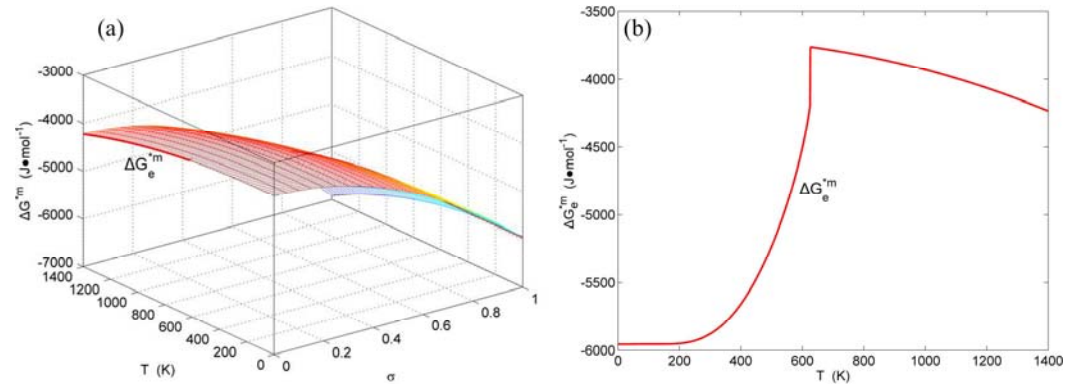

Fig. B.2 EHNP charts with EHNP curve of first order thermodynamic properties on disordering $Au_3Cu((A_4^{Au})_3A_0^{Cu})$: (a) Three-dimensional mixedal characteristic Gibbs energy $\Delta G^{*m}-T-\sigma$ EHNP chart with $\Delta G_{e}^{*m}-T$ path; (b) $\Delta G_{e}^{*m}-T$ path

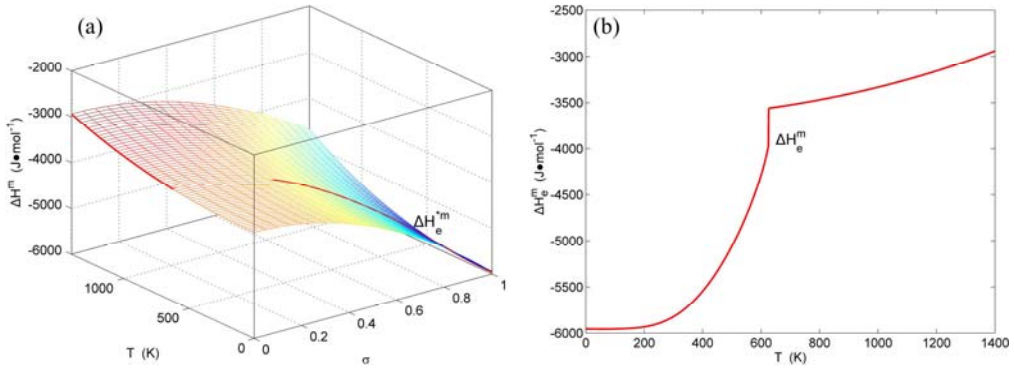

Fig. B.3 EHNP charts with EHNP curve of first order thermodynamic properties on disordering $Au_3Cu((A_4^{Au})_3A_0^{Cu})$: (a) Three-dimensional mixed enthalpy $\Delta H^{m}-T-\sigma$ EHNP chart with $\Delta H_{e}^{m}-T$ path; (b) $\Delta H_{e}^{m}-T$ path

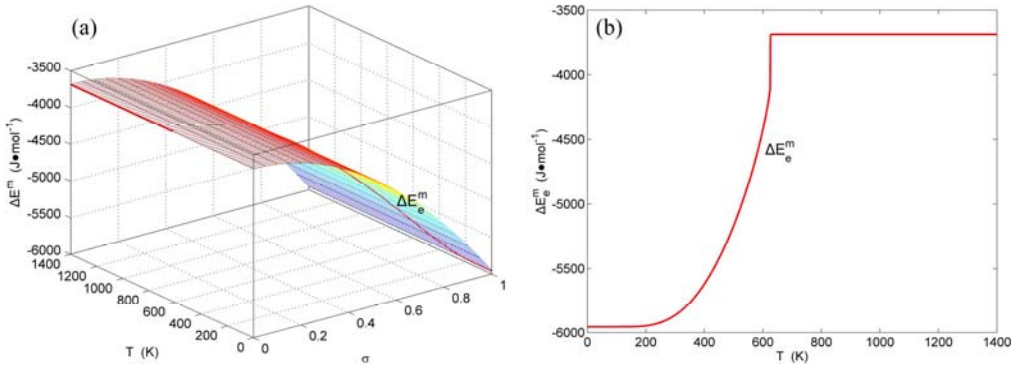

Fig. B.4 EHNP charts with EHNP curve of first order thermodynamic properties on disordering $Au_3Cu((A_4^{Au})_3A_0^{Cu})$: (a) Three-dimensional mixed potential energy $\Delta E^{m}-T-\sigma$ EHNP chart with $\Delta E_{e}^{m}-T$ path; (b) $\Delta E_{e}^{m}-T$ path

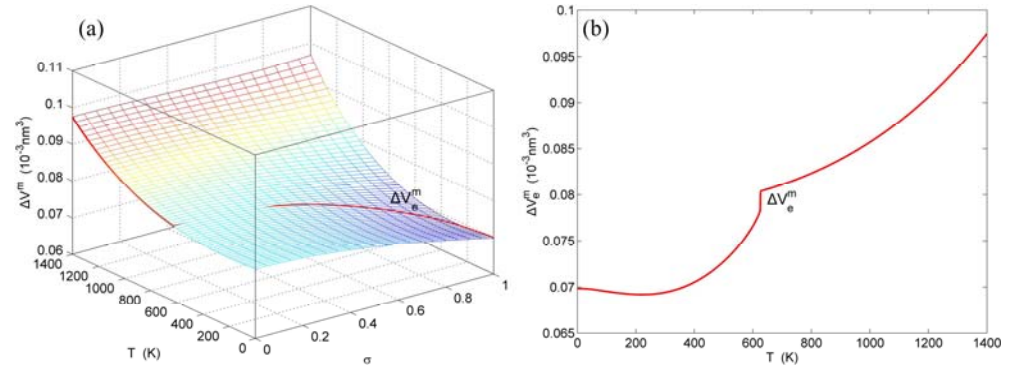

Fig. B.5 EHNP charts with EHNP curve of first order thermodynamic properties on disordering $Au_3Cu((A_4^{Au})_3A_0^{Cu})$: (a) Three-dimensional mixed volume $\Delta V^{m}-T-\sigma$ EHNP chart with $\Delta V_{e}^{m}-T$ path; (b) $\Delta V_{e}^{m}-T$ path

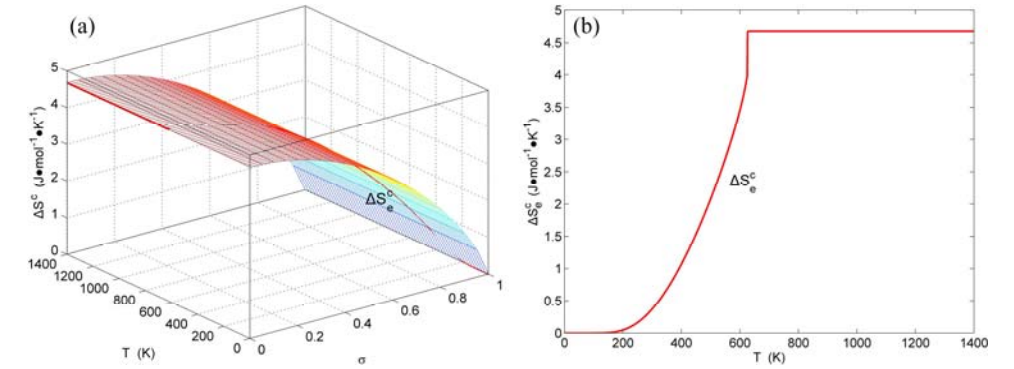

Fig. B.6 EHNP charts with EHNP curve of first order thermodynamic properties on disordering $Au_3Cu((A_4^{Au})_3A_0^{Cu})$: (a) Three-dimensional configurational entropy $S^{c}-T-\sigma$ EHNP chart with $S_{e}^{c}-T$ path; (b) $S_{e}^{c}-T$ path

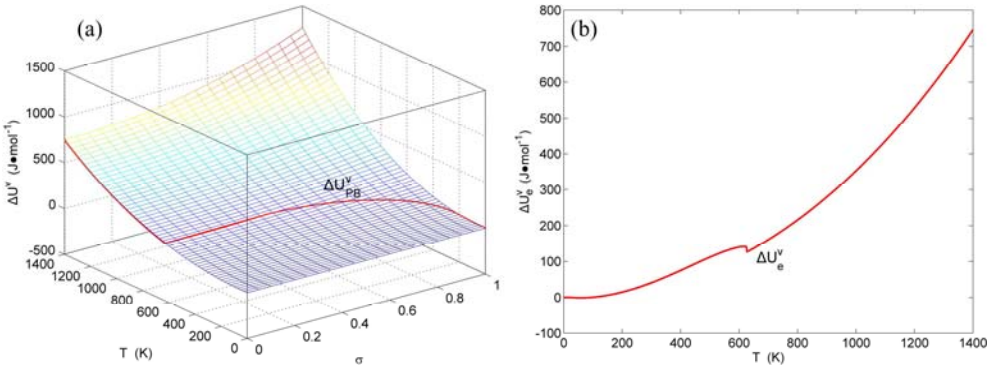

Fig. B.7 EHNP charts with EHNP curve of first order thermodynamic properties on disordering $Au_3Cu((A_4^{Au})_3A_0^{Cu})$: (a) Three-dimensional generalized vibration energy $\Delta U^{m.v}-T-\sigma$ EHNP chart with $\Delta U_e^{m.v}-T$ path; (b) $\Delta U_e^{m.v}-T$ path

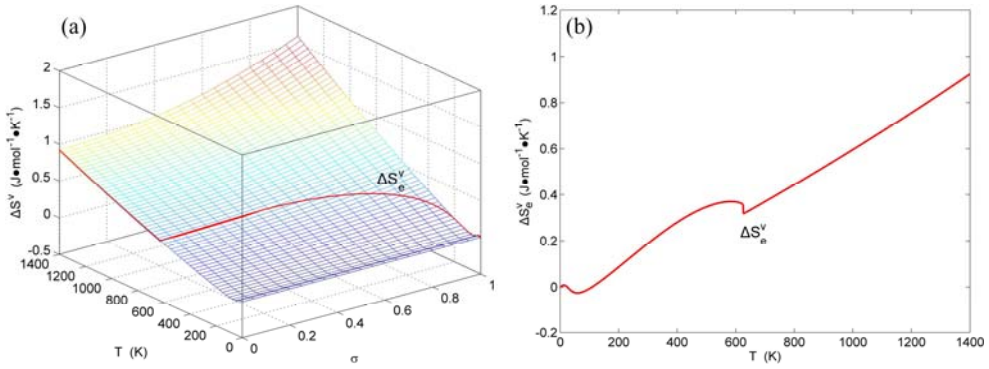

Fig. B.8 EHNP charts with EHNP curve of first order thermodynamic properties on disordering $Au_3Cu((A_4^{Au})_3A_0^{Cu})$: (a) Three-dimensional generalized vibration entropy $\Delta S^{v}-T-\sigma$ EHNP chart with $\Delta S_e^{v}-T$ path; (b) $\Delta S_e^{v}-T$ path

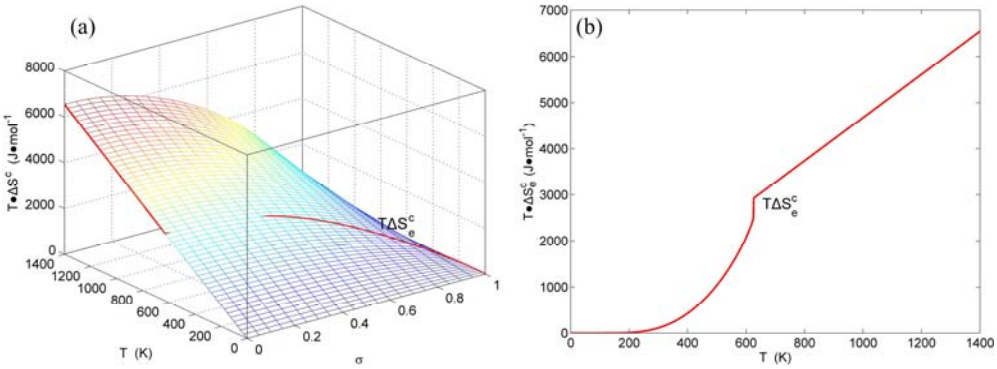

Fig. B.9 EHNP charts with EHNP curve of first order thermodynamic properties on disordering $Au_3Cu((A_4^{Au})_3A_0^{Cu})$: (a) Three-dimensional configurational entropy energy $TS^{c}-T-\sigma$ EHNP chart with $TS_e^{c}-T$ path; (b) $TS_e^{c}-T$ path

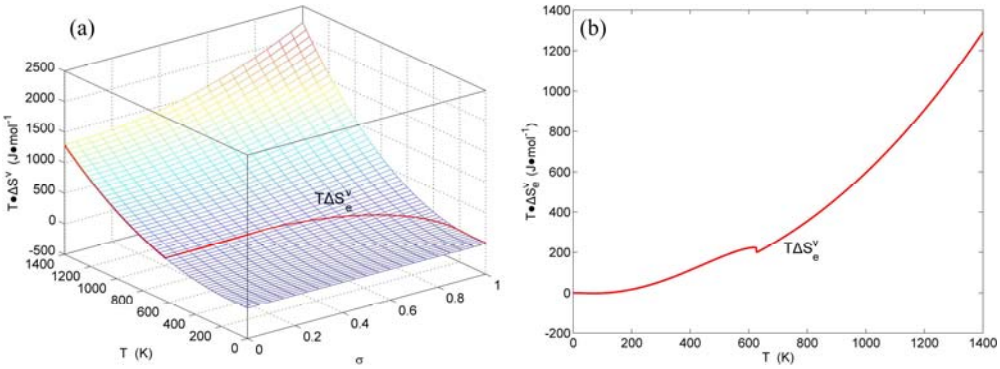

Fig. B.10 EHNP charts with EHNP curve of first order thermodynamic properties on disordering $Au_3Cu((A_4^{Au})_3A_0^{Cu})$: (a) Three-dimensional generalized vibration entropy energy $T\Delta S^{v}-T-\sigma$ EHNP chart with $T\Delta S_e^{v}-T$ path; (b) $T\Delta S_e^{v}-T$ path

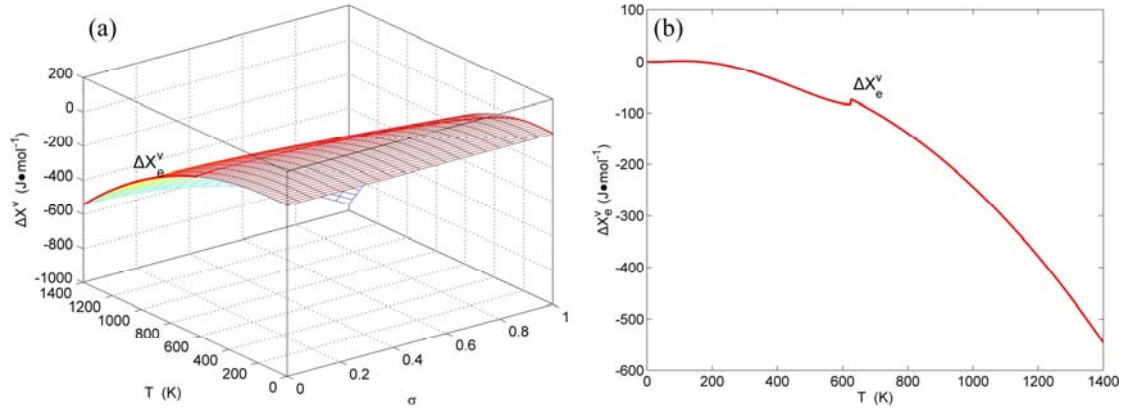

Fig. B.11 EHNP charts with EHNP curve of first order thermodynamic properties on disordering $Au_3Cu((A_4^{Au})_3A_0^{Cu})$: (a) Three-dimensional generalized vibration free energy $\Delta X^{v}-T-\sigma$ EHNP chart with $\Delta X^{v}_{e}-T$ path; (b) $\Delta X^{v}_{e}-T$ path

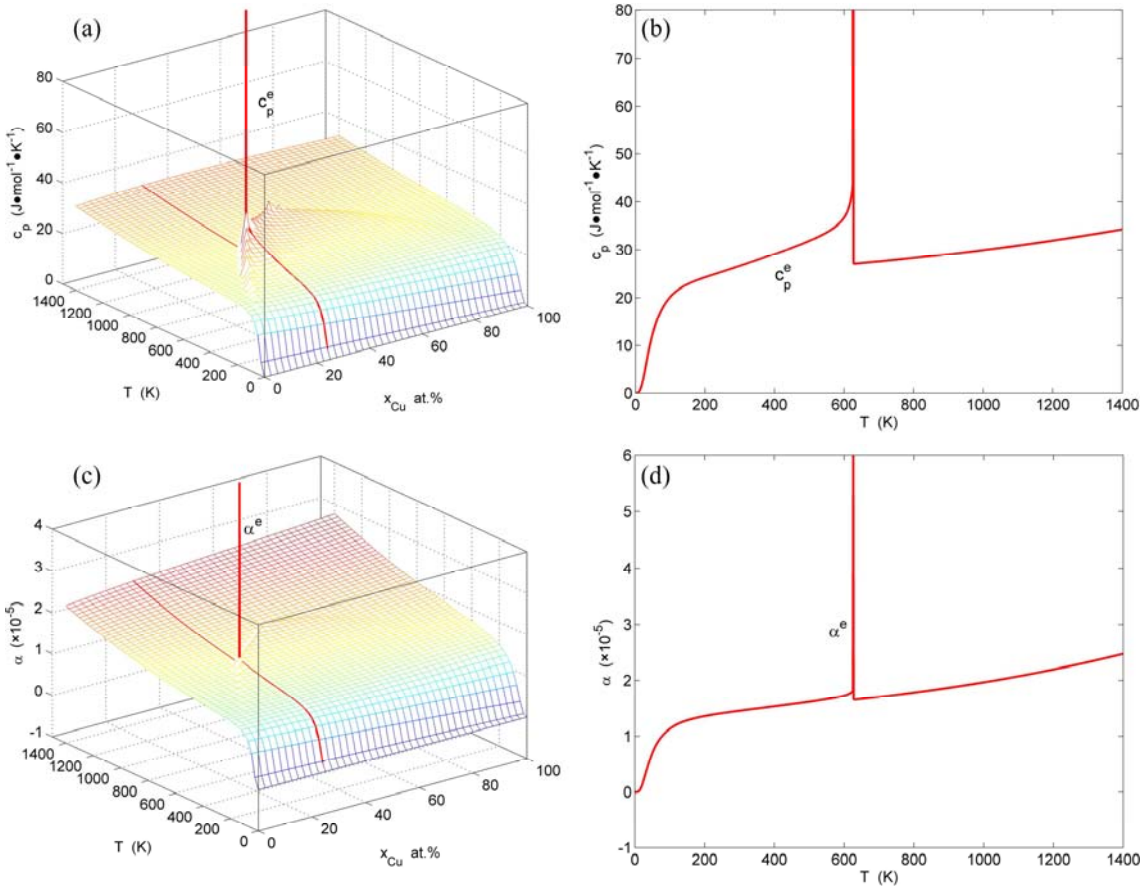

Fig. B.12 Second order thermodynamic properties (heat capacity and thermal expansion coefficient) on disordering $Au_3Cu((A_4^{Au})_3A_0^{Cu})$: (a) $c_p^{e}-T$ path on c_p-x-T EHNP diagram; (b) $c_p^{e}-T$ path; (c) $\alpha^{e}-T$ path on $\alpha-x-T$ EHNP chart; (d) $\alpha^{e}-T$ path (These charts are calculated by temperature step ΔT =1 K and order degree step $\Delta\sigma$ =0.00001)

C Difference method of Gibbs energies between ordered and disordered phases

The $\Delta G^{m}_{PB}(x,T)$-phase boundary curve of Au_3Cu-type sublattice system has been obtained by the difference method of Gibbs energies between ordered Au_3Cu-type phase and disordered phase (see Fig. C.1). It has been proved that there is no two-phase region of the ordered and disordered phases, because ordered and disordered alloys belong in the same fcc-based lattice Au−Cu system.

D Other thermodynamic properties EHNP diagrams

According to $x_i^{Au}-x-T$ and $x_i^{Cu}-x-T$ EHNP diagrams obtained from $\Delta G^{m}-x-T$ diagram, we have obtained other $q-x-T$ EHNP diagrams of $AuCu_3$-type sublattice system shown in Figs. D.1 and D.2. It

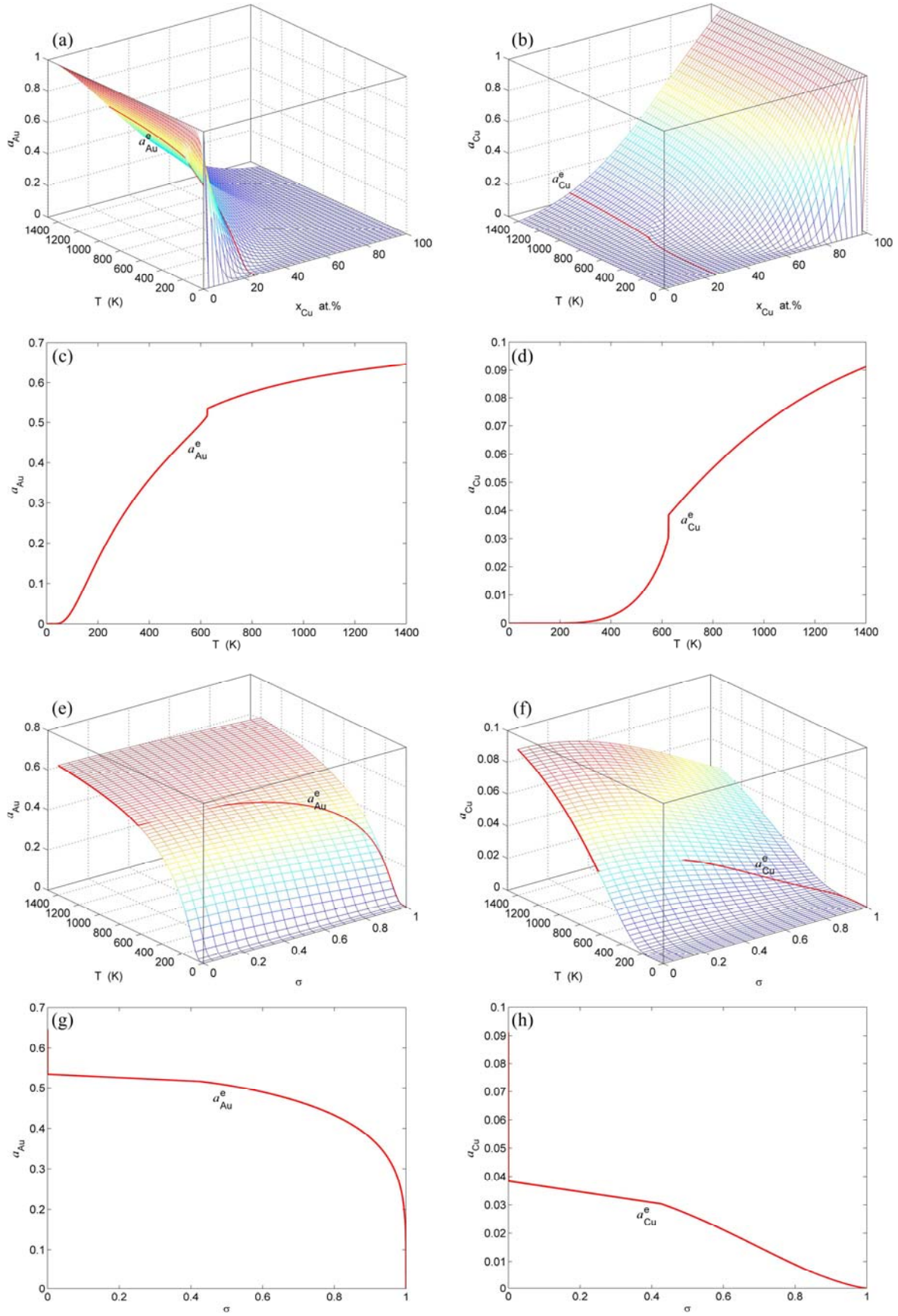

Fig. B.13 Activities on disordering $Au_3Cu((A_4^{Au})_3A_0^{Cu})$: (a, b) $a_{Au}^{e}-T$ and $a_{Cu}^{e}-T$ paths on $a_{Au}-x-T$ and $a_{Cu}-x-T$ EHNP diagrams; (c, d) $a_{Au}^{e}-T$ and $a_{Cu}^{e}-T$ paths; (e, f) $a_{Au}^{e}-T$ and $a_{Cu}^{e}-T$ paths on $a_{Au}-T-\sigma$ and $a_{Cu}-T-\sigma$ EHNP charts; (g, h) $a_{Au}^{e}-\sigma$ and $a_{Cu}^{e}-\sigma$ paths

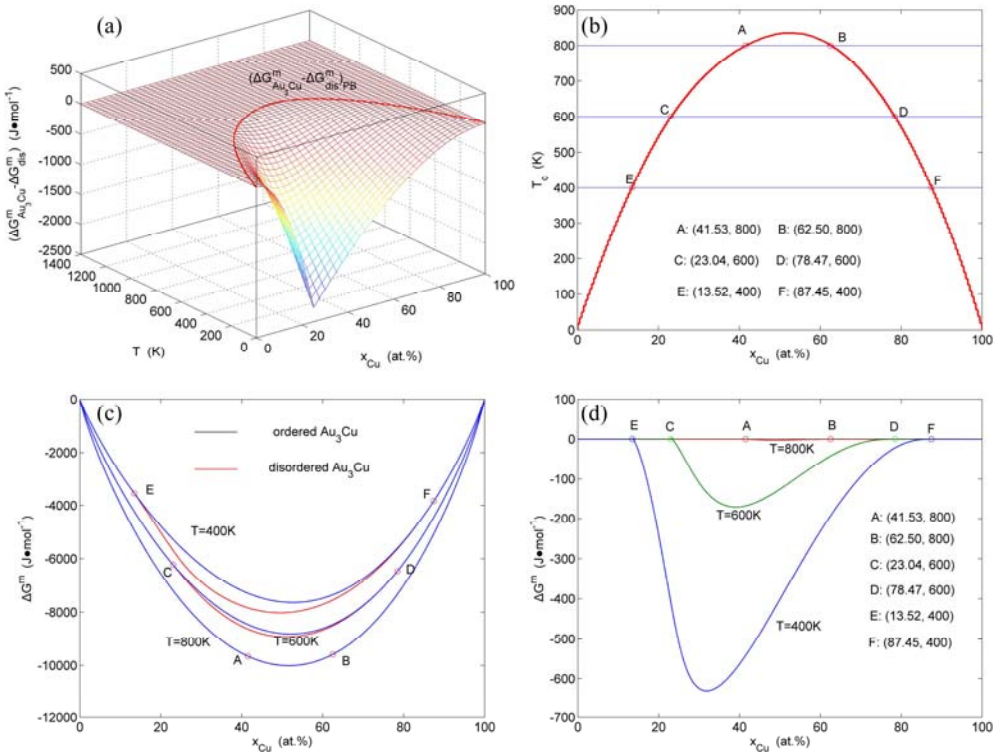

Fig. C.1 Difference method for calculating phase boundary curve of Au_3Cu-type sublattice system: (a) Three-dimensional ($\Delta G^{m}_{ord.}-\Delta G^{m}_{dis.}$) diagram with phase boundary $\Delta G^{m}_{PB}(x,T)$- curve; (b) Phase boundary $T_{PB}(x)$- curve; (c) $\Delta G^{m}_{ord.}$- and $\Delta G^{m}_{dis.}$- curves at 400 K, 600 K and 800 K as a function of composition; (d) Difference values of $\Delta G^{m}_{ord.}-\Delta G^{m}_{dis.}$ at 400 K, 600 K and 800 K as a function of composition

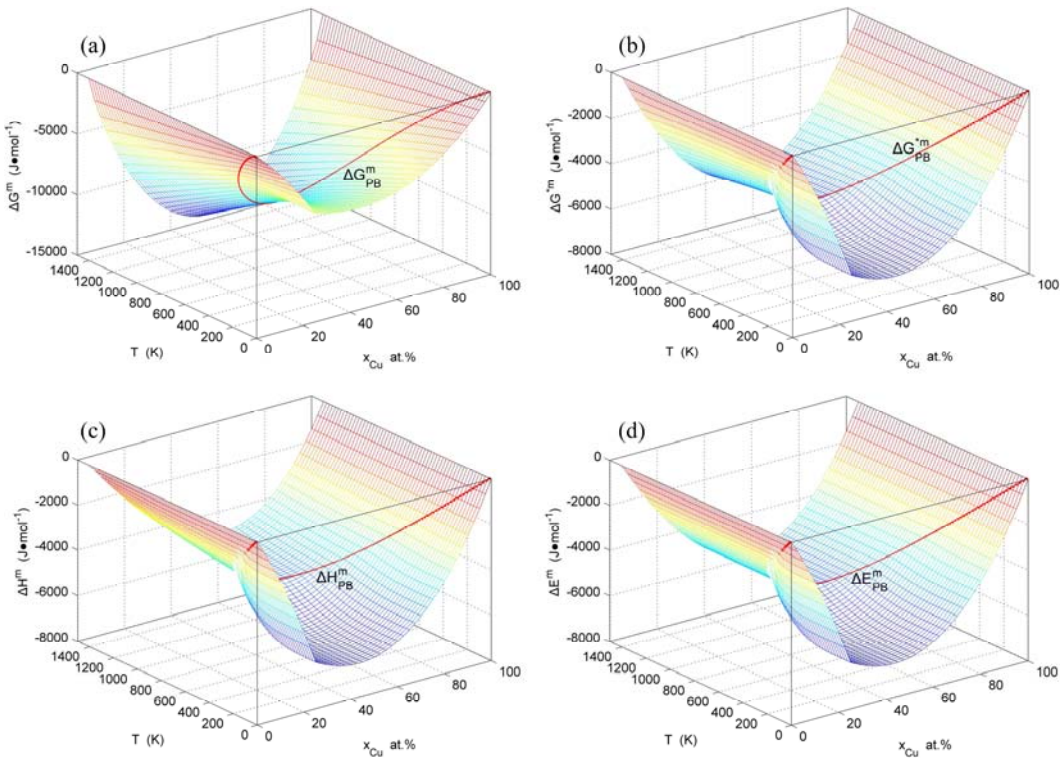

Fig. D.1 $q-x-T$ EHNP diagrams of Au_3Cu-type sublattice system: (a) Mixed Gibbs energy $\Delta G^{m}-x-T$ three-dimensional EHNP diagram; (b) Mixed characteristic Gibbs energy $\Delta G^{*m}-x-T$ three-dimensional EHNP diagram, without configuration entropy; (c) Mixed enthalpy $\Delta H^{m}-x-T$ three-dimensional EHNP diagram; (d) Mixed potential energy $\Delta E^{m}-x-T$ three-dimensional EHNP diagram, without variations in AG-potential energies with temperatures

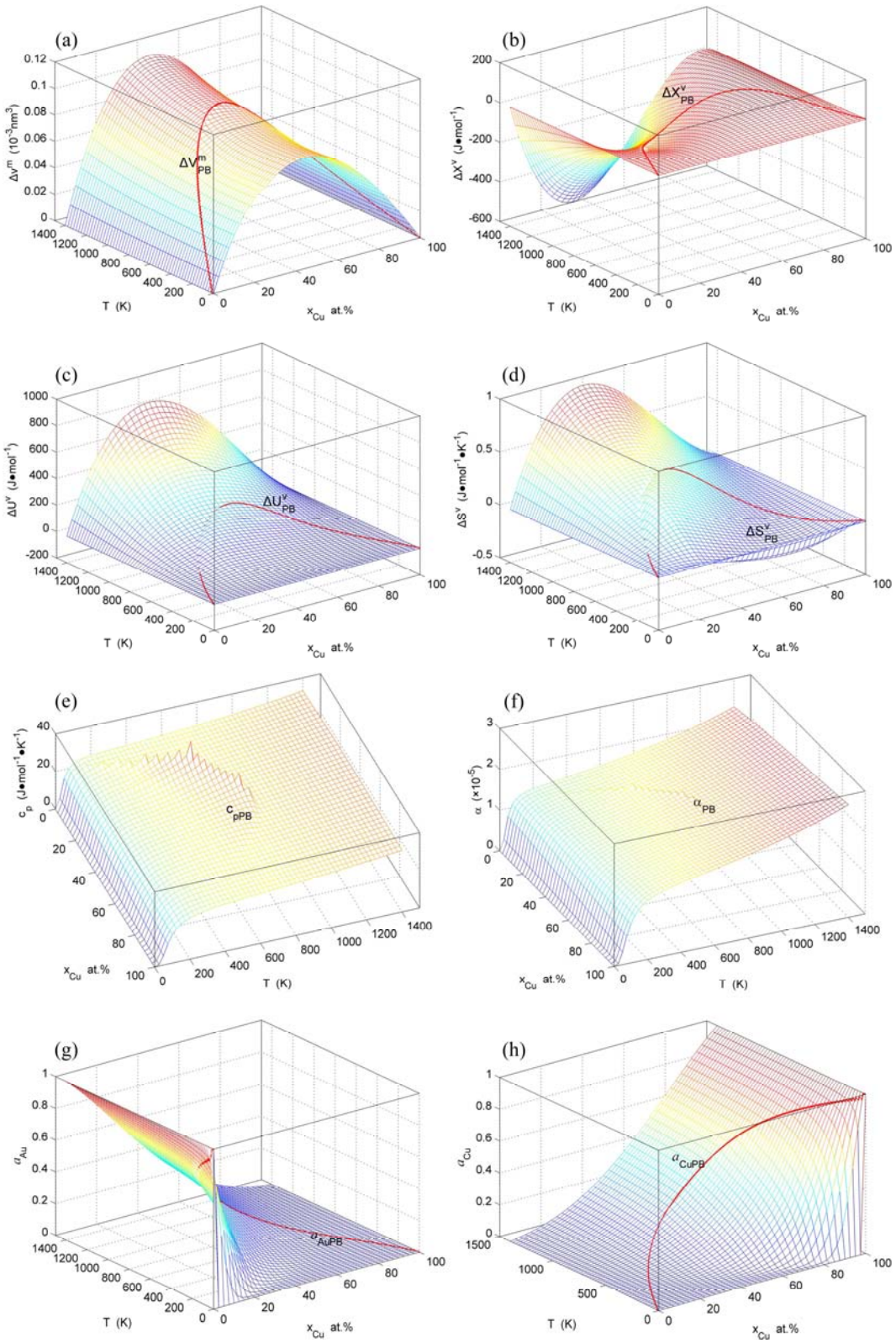

Fig. D.2 $q-x-T$ EHNP diagrams of Au_3Cu-type sublattice system: (a) Mixed volume $\Delta V^{m}-x-T$ three-dimensional EHNP diagram; (b) Generalized mixed vibration free energy $\Delta X^{v}-x-T$ three-dimensional EHNP diagram; (c) Generalized mixed vibration energy $\Delta U^{v}-x-T$ three-dimensional EHNP diagram, including variations in AG-potential energies with temperatures; (d) Generalized mixed vibration entropy $\Delta S^{v}-x-T$ three-dimensional EHNP diagram; (e) Heat capacity $c_p^{m}-x-T$ three-dimensional EHNP diagram; (f) Thermal expansion coefficient $\alpha-x-T$ three-dimensional EHNP diagram; (g) $a_{Au}-x-T$ three-dimensional diagram; (h) $a_{Cu}-x-T$ three-dimensional diagram

should be emphasized that from each three-dimensional $q-x-T$ EHNP diagram, we can obtain isocompositional q_x-T, isoproperty T_q-x and isothermal q_T-x path phase diagrams. These diagrams are interconnected to form a big database about structure, properties and their variations with temperature of alloy systems. Therefore, the man's knowledge of relationships of structure, properties and environments for alloy systems has been changed from single causality to systematic correlativity.

References

[1] XIE You-qing, LI Xiao-bo, LIU Xin-bi, NIE Yao-zhuang, PENG Hong-jian. Alloy gene Gibbs energy partition function and equilibrium holographic network phase diagrams of AuCu-type sublattice system [J]. International Journal of Communications, Network and System Sciences, 2013, 12(6): 415−442.

[2] XIE You-qing. Systematic science of metallic materials [M]. Changsha: Central South University of Technology Press, 1998. (in Chinese)

[3] XIE You-qing. Systematic science of alloys [M]. Changsha: Central South University Press, 2012. (in Chinese)

[4] XIE You-qing. Atomic energies and Gibbs energy functions of Ag−Cu alloys [J]. Science in China, Series E: Technological Science, 1998, 41(2): 146−156.

[5] XIE You-qing, ZHANG Xiao-dong. Atomic volumes and volume functions of Ag−Cu alloys [J]. Science in China, Series E: Technological Science, 1998, 41(2): 157−168.

[6] XIE You-qing. A new potential function with many-atom interactions in solid [J]. Science in China, Series A, 1993, 36(1): 90−99.

[7] XIE You-qing. Electronic structure and properties of pure iron [J]. Acta Metallargics et Materialia, 1994, 42(11): 3705−3715.

[8] XIE You-qing, LIU Xin-bi, PENG Hong-jian, NIE Yao-zhuang, LI Xiao-bo, LI Yan-feng. Characteristic atom arranging crystallography of alloy phases for Au−Cu system [J]. Science China: Technological Sciences, 2011, 54(6): 1560−1567.

[9] XIE You-qing, PENG Kun, LIU Xin-bi. Influences of x_{Ti}/x_{Al} atomic states, lattice constants and potential-energy planes of ordered fcc TiAl type alloys [J]. Physica B, 2004, 344(1−4): 5−20.

[10] XIE You-qing, LIU Xin-bi, PENG Kun. Atomic states, potential energies, volumes, stability and brittleness of ordered fcc $TiAl_3$ type alloys [J]. Physica B, 2004, 353(1−2): 15−33.

[11] XIE You-qing, PENG Hong-jian, LIU Xin-bi, PENG Kun. Atomic states, potential energies, volumes, stability and brittleness of ordered fcc Ti_3Al type alloys [J]. Physica B, 2005, 362(1−4): 1−17.

[12] XIE You-qing, TAO Hui-jin, PENG Hong-jian, LIU Xin-bi, PENG Kun. Atomic states, potential energies, volumes, stability and brittleness of ordered fcc $TiAl_2$ type alloys [J]. Physica B, 2005, 366(1−4): 17−37.

[13] XIE You-qing, PENG Hong-jian, LIU Xin-bi, LI Xiao-bo, NIE Yao-zhuang. New atom movement mechanism for tracking path on disordering AuCuI($A_8^{Au}A_4^{Cu}$) compound [J]. Transactions of Nonferrous Metals Society of China, 2014, 24(10): 3321−3256.

[14] XIE You-qing, LI Xiao-bo, LIU Xin-bi, NIE Yao-zhuang, PENG Hong-jian. Alloy gene Gibbs energy partition function and equilibrium holographic network phase diagrams of $AuCu_3$-type sublattice system [J]. Transactions of Nonferrous Metals Society of China, 2014, 24(11): 3585−3610.

[15] SPRUŠIL B, PFEILER W. The retro-effect in stoichiometric CuAu: A resistometric study [J]. Intermetallics, 1997, 5(7): 501−505.

[16] PFEILER W, SPRUŠIL B. Atomic ordering in alloys: Stable states and kinetics [J]. Materials Science and Engineering A, 2002, 324(1−2): 34−42.

[17] SPRUŠIL B, CHALUPA B. Checking the model for dynamic disordering in CuAu [J]. Materials Science and Engineering A, 2002, 324(1−2): 58−61.

[18] FOWLER R H, GUGGENHEIM E A. Statistical thermodynamics [M]. Cambridge: Cambridge University Press, 1937.

[19] MAYER J E, MAYER M G. Statistical mechanics [M]. New York: Wiley, 1940.

[20] GUGGENHEIM E A. Mixtures [M]. Oxford: Oxford University Press, 1952.

[21] PRIGOGINE I. Molecular theory of solutions [M]. Amsterdam: North Holland, 1957.

[22] HILL T L. Introduction to statistical thermodynamics [M]. Reading, MA: Addison-Wesley, 1960.

[23] XIE You-qing, ZHANG Xiao-dong. Electronic structures of Ag−Cu alloys [J]. Science in China, Series E: Technological Science, 1998, 41(3): 225−236.

[24] KIKUCHI R, de FONTAINE D, MURAKAMI M, NAKAMURA T. Ternary phase diagram calculations—II Examples of clustering and ordering systems [J]. Acta Metallurgica, 1997, 25(2): 207−219.

[25] SUNDMAN B, FRIES S G, OATES W A. A thermodynamic assessment of the Au−Cu system [J]. CALPHAD, 1998, 22(3): 335−354.

[26] SUNDMAN B, FRIES S G, OATES W A. A calphad assessment of the Au−Cu system using the cluster variatiation method [J]. Z Metallkd, 1999, 90(5): 267−273.

[27] CAO W, CHANG Y A, ZHU J, CHEN S, OATES W A. Thermodynamic modeling of the Cu−Ag−Au system using the cluster/site approximation[J]. Intermetallics, 2007, 15(8): 1438−1446.

[28] OZOLINŠ V, WOLVERTON C, ZUNGER A. Cu−Au, Ag−Au, Cu−Ag, and Ni−Au Intermetallics: First-principles study of temperature-composition phase diagrams and structures [J]. Physical Review B, 1998, 57(12): 6427−6443.

[29] ASTA M, de FONTAINE D. First-principles study of phase stability of Ti−Al intermetallic compounds [J]. J Mater Res, 1993, 8(10): 2554−2568.

[30] DINSDALE A T. SGTE data for pure elements [J]. CALPHAD, 199l, 15(4): 317−425.

[31] KAUFMAN L, ÅGREN J. First and second generation-birth of the materials genome [J]. Scripta Materialia, 2014, 70(1): 3−6.

[32] BRAGG W L, WILLIAMS E J. The effect of thermal agitation on atomic arrangement in alloys [J]. Proceedings the royal of society A, 1934, 145(2): 699−730.

[33] BRAGG W L, WILLIAMS E J. The effect of thermal agitation on atomic arrangement in alloys II [J]. Proceedings the Royal of Society A, 1935, 51(4): 540−566.

[34] XIE You-qing, MA Liu-ying, ZHANG Xiao-dong, ZHOU Ping, ZHAO Li-ying. Microstructure and properties of Cu−Ni alloy [J]. Science in China, Series A, 1993, 36(5): 612−623.

[35] OATES W A, ZHANG F, CHEN S L, CHANG Y A. Improved cluster-site approximation for the entropy of mixing in multicomponent solid solutions [J]. Physical Review B, 1999, 59(17): 11221−11225.

[36] WEI S H, MBAYE A A, FERRIRA L G, ZUNGER A. First-principles calculations of the phase diagrams of noble metals: Cu−Au, Cu−Ag and Ag−Au [J]. Phys Rev B, 1987, 36(20): 4163−4185.

[37] LU H S, LIANG C K. The superlattice formation and lattice spacing changes in copper−gold alloys [J]. Acta Physica Sinica, 1966, 22(6): 659−697. (in Chinese)

[38] LU H S, LIANG C K. The existence of the superlattice $CuAu_3$ in the Cu−Au system [J]. Science Bulletin, 1966, 17(9): 395−396.

[39] LU H S, LIANG C K. Experimental evidence of order-disorder

transitions as of the second degree [J]. Science Bulletin, 1966, 17(10): 441−443.

[40] XIE You-qing, LI Yan-fen, LIU Xin-bi, LI Xiao-bo, PENG Hong-jian, NIE Yao-zhuang. Characteristic atom occupation patterns of Au_3Cu, $AuCu_3$, AuCuI and AuCuII based on experimental data of disordered alloys [J]. Transactions of Nonferrous Metals Society of China, 2011, 21(5): 1092−1104.

[41] XIE You-qing, NIE Yao-zhuang, LI Xiao-bo, LIU Xin-bi, PENG Hong-jian, LI Yan-fen. Characteristic atom potential energy partition function of Au_3Cu type ordered alloys in FP-SSA framework [J]. The Chinese Journal of Nonferrous Metals, 2011, 21(10): 2489−2501. (in Chinese)

Au_3Cu-亚格子系统的合金基因 Gibbs 能配分函数和平衡全息网络相图

谢佑卿[1,2,3], 聂耀庄[4], 李小波[5], 彭红建[6], 刘心笔[1,2,3]

1. 中南大学 材料科学与工程学院，长沙 410083；
2. 中南大学 粉末冶金研究院，长沙 410083；
3. 中南大学 粉末冶金国家重点实验室，长沙 410083；
4. 中南大学 物理与电子学院，长沙 410083；
5. 湘潭大学 材料科学与工程学院，湘潭 411105；
6. 中南大学 化学化工学院，长沙 410083

摘　要：以 Au_3Cu-亚格子系统为例，介绍了 3 项发现：第一，至今阻碍金属材料科学进步的第四大障碍是研究者们尚未认识到一个真正的合金相 Gibbs 能函数应由合金基因序列和它们自己的 Gibbs 能级序列构建的 Gibbs 能配分函数导出。第二，建立合金基因 Gibbs 能配分函数的六条规则，特别证明了计算合金组态熵的简并因子中结构单元占居 Gibbs 能级的概率应按照组元占居格点的概率方式简并；第三，以前研究者从未预料到的主要特征：具有一条没有有序相和无序相共存区的单相相界线；相界线顶点成分和温度远偏离 Au_3Cu 化合物临界点的成分和温度；在 0 K 时，Gibbs 能随成分变化曲线上的最低点成分远偏离 Au_3Cu 化合物的成分；Au_3Cu-型长程有序合金的理论极限成分范围由第一跳变有序度决定。

关键词：Au_3Cu 化合物；Au_3Cu-型亚格子系统；合金基因 Gibbs 能配分函数；平衡全息网络相图；系统金属材料科学

(Edited by Yun-bin HE)